PRELIMINARY DESIGN OF A SATELLITE-LAUNCHED MANNED VEHICLE FOR EXPLORATION OF THE SURFACE OF THE PLANET MARS

by

Norman L. Donaldson no degree
Dennis C. Posey
Richard J. Talbot
Dennis K. Ward

SUBMITTED IN PARTIAL FULFILLMENT OF THE
REQUIREMENTS FOR THE DEGREE OF
BACHELOR OF SCIENCE

at the

MASSACHUSETTS INSTITUTE OF TECHNOLOGY

1959

Signatures of Authors Signature redacted

Signature redacted

Signature redacted

Signature redacted

Dept. of Aeronautical Engineering, May 25, 1959

Certified by Signature redacted

Thesis Supervisor

Aero
Thesis
1959

p. 8

ABSTRACT

The object of this thesis is the design of a manned vehicle capable of descending from an established circum-Martian orbit to the surface of the planet, landing two observers plus necessary equipment on the face of the planet for a specified amount of time, and then returning them to the manned satellite in orbit. The vehicle is capable of this requirement only--it is not capable of interplanetary travel.

The ascent vehicle which returns to orbit is carried down to the planet's surface on a hypersonic delta wing capable of entry into the atmosphere and landing on the surface. Once the wing has landed, the ascent vehicle is then capable of being erected into a vertical position for firing into orbit. All special equipment needed for the landing, survival of the personnel while on the surface, and exploration of the surface is carried in the wing. This and the entire wing structure is then abandoned on the surface. Only equipment needed for the ascent, samples, and the personnel are returned to the satellite orbit.

ACKNOWLEDGEMENTS

The authors would like to express their sincere thanks to our instructors, our classmates, and the numerous people who have given much helpful advice. In particular we thank Prof. Eugene Larrabee for his suggestions on solutions to entry problems, and wings; Prof. Paul E. Sandorff for suggesting this thesis topic and for his ideas on configuration and structure, Jack Parmley for helping with the calculations of the chemical properties of the propellants; Lee Friar for help with the graphs, Burnell West for his typing; and Richard Winkler for his help with the difficult task of reproduction.

TABLE OF CONTENTS

FIGURES

LOGISTIC REQUIREMENTS OF A MANNED MARS MISSION

The general expedition to Mars is assumed to be comprised of the following logistic requirements: (Ref. 25 & 8)

1. Launching supplies and equipment to construct a manned satellite around the earth.

2. Constructing ships to travel to a satellite orbit around Mars. These ships would carry all necessary payload needed for the actual descent to the planet.

3. A separate vehicle would then descend from the established Mars orbit, land on the surface, remain for a specified time and then return to the satellite ships in orbit.

4. These landing ships would then be abandoned in the circum-Martian orbit, along with any other unnecessary weight, and the mother ships would then return to the previously established Earth satellite orbit or perhaps a higher orbit. For a higher orbit a specially designed relief ship would return personnel and equipment to the earth or the lower orbit.

In Ref. 25, von Braun has worked out what might be aptly called an "invasion" of Mars. He has calculated rough logistic requirements for a complete expedition on the grandious scale. The cost of his expedition would equal or exceed the cost of the Korean War, and it is questionable whether any government would embark on a financial venture of this magnitude of their own volition. For this reason we have done our calculations of the landing vehicle assuming a much smaller mission requirement. A first manned mission is probably possible by the year 2000 A.D. (See Appendix I) This mission would probably consist of 8-12 people and two or three landing craft, each capable of landing two people on the surface of the planet. It is desirable for each of these landing vehicles to be capable of remaining on the surface for a maximum of 30 days. (See Appendix VI) This is considered to be an optimum with respect to payload weight and consequent required fuel considerations. Using two or more landing vehicles increases the probability of mission success. Also, it permits exploring several regions of the planet's surface.

CIRCUM-MARTIAN ORBIT REQUIREMENTS

It is desirable to establish the circum-Martian orbit such that the propulsion requirements for the entire mission are a minimum. This is impossible to evaluate analytically unless the detail design of each vehicle for each part of the mission is know. Since the weight of the landing vehicles will probably be small in comparison to the weight of the mother satellite vehicles, it is assumed that this optimum can be represented by the specific circum-Martian orbit which optimizes the transfer from the Earth orbit to the Mars
orbit which optimizes the transfer from the Earth orbit to the Mars
orbit and return. According to Ehricke (Ref. 56), this optimum radius from the center of Mars is 3525 n. mi. at an altitude of 1695 n. mi.

p. 8

IDEAL VELOCITY REQUIREMENTS OF ENTRY VEHICLE

The vehicle has previously entered the circum-Martian orbit as indicated on Fig. 1a. In order to transfer from the circular orbit to the altitude for entry, a Hohmann elliptical transfer maneuver is necessary. This maneuver assumes the net effect of applying thrust tangent to the vehicle's flight path is an incremental change in the velocity. This is valid because of the relatively short path over which the retro-rockets burn. This thrusting maneuver is accomplished in two parts, first a retarding thrust, Δv_1 is applied to get the vehicle into the elliptical transfer orbit. When it comes tangent to the desired entry orbit (180° diametrically opposed to the first thrusting maneuver) another retarding thrust maneuver, Δv_2 is applied to retard the vehicle's velocity to that needed for a circular satellite orbit at that altitude. This puts the vehicle into its entry phase with essentially zero angle to the atmosphere. The incremental velocities necessary can be calculated from satellite velocities for circular orbits, and velocities of the elliptical transfer orbit at apogee and perigee. The values of these parameters are:

R_e = 1902.2 n. mi. entry
h_e = 700,000 ft. = 115.2 n. mi.
$R_♂$ = 1787 n. mi. ♂
R_s = 3482 n. mi.
h_s = 1695 n. mi.

The ideal velocity requirements are calculated as follows:

$$(v_S)_{R_S} = \sqrt{\frac{GM}{R_S}} \tag{1a}$$

$$v_{\pi} = \sqrt{\frac{r_{\alpha}}{r_{\pi}}}\sqrt{\frac{2GM}{r_{\alpha}+r_{\pi}}} \tag{2a}$$

$$v_{\alpha} = \sqrt{\frac{r_{\pi}}{r_{\alpha}}}\sqrt{\frac{2GM}{r_{\alpha}+r_{\pi}}} \tag{3a}$$

$$\Delta v_1 = (v_S)_{RS} - (v_{\alpha})_{TRANS.} \tag{4a}$$

$$\Delta v_2 = (v_{\pi})_{TRANS} - (v_S)_{Re} \tag{5a}$$

$r_{\alpha} + r_{\pi} = R_S + R_e = 5384.3$ n. mi.

$v_{\pi} =$	13,030 ft/sec	$\Delta v_1 =$	1,335 ft/sec
$v_{\alpha} =$	7,125 ft/sec	$\Delta v_2 =$	1,570 ft/sec
$(v_S)_{R_S} =$	8,460 ft/sec		
$(v_S)_{R_e} \doteq$	11,460 dt/sec	$\Delta v_{TOTAL} =$	2,905 ft/sec

IDEAL VELOCITY REQUIREMENTS OF ASCENT VEHICLE

This vehicle will have to make a similar transfer to return to the 1695 n. mi. altitude orbit. However, this time the transfer will be from the surface of the planet to the orbit. Drag and gravity terms will now become important due to the fact that the ascent vehicle will be launched vertically. The gravity and the drag terms are nasty to handle because they involve a numerical integration. Therefore, these will be evaluated by comparison with known data on existing missiles. Ref. 80 gives some of this data.

The values of the velocities are:

v_{π} = 13,650 ft/sec v_{ORBIT} = 8480 ft/sec

v_{α} = 7,200 ft/sec $v_{CIRC.}$ = 775 ft/sec

$\Delta v_1 = v_{\pi} - v_{CIRC} =$	13,650 - 775 =	12, 875 ft/sec
$\Delta v_2 = v_{ORBIT} - v_{\alpha}$	= 8,480 -7,200 =	1, 280 ft/sec
		14, 155 ft/sec
estimated drag losses		1, 300
10% allowance for maneuvering		1, 416
		16, 871 ft/sec
gravity losses		629
Total Velocity Req.		17, 500 ft/sec

WEIGHT ESTIMATES FROM IDEAL VELOCITY REQUIREMENTS

The total velocity requirements for the ascent vehicle easily give us the required mass ratio, MR necessary for the vehicle by:

$$v_p \cong \bar{c} \ln MR \qquad MR = \frac{W_o}{W_f} = \frac{\text{Initial weight}}{\text{Final weight}} = \frac{m_o}{m_o - m_p} \quad (6a)$$

MR = 6.6

It has been specified (Appendices III & V) that we will be bringing down 2500 lbs. payload from orbit, and will return a payload of 700 lbs. to orbit. From Ref. 78 & 81 it was possible to determine the structural factor needed for a satellite launching vehicle on the surface of Mars. Adding a safety factor to include the additional weight of structure needed for the crew cabin, and to take the transverse loading, we obtained a structural factor, $\epsilon = 0.10$. This was then used to calculate the weight of the ascent vehicle. The wing area of a wing necessary to land this load was then calculated.

The detailed breakdown of the weight of the ascent vehicle is:

W_i	13,500 lb.	M_i	419.5 slugs
W_{PL}	700	M_{PL}	21.7
W_s	1,345	M_s	41.8
W_P	11,455	M_P	356.0

The weight of the wing structure was estimated by careful consideration of the gravity of Mars, and comparison with existing wing structures that are used here on Earth. The detailed Breakdown of the weight of the wing is:

W_i	4,500lb.	M_i	139.9 slugs
W_{PL}	1,800	M_{PL}	56.0
W_s	2,700	M_s	83.9

The detailed breakdown of the weight of both vehicles together for orbital descent is:

W_i	18,000 lb.	M_i	559.4 slugs
W_{PL}	2,500	M_{PL}	77.7
W_s	4,045	M_s	125.7
W_P	11,455	M_P	356.0

Data on descent vehicle:

Wing area	A	800 sq. ft.
Root chord	c_r	46.2 ft.
Span	b	34.6 ft.
Mean Aero. chord	M.A.C.	30.8 ft.
Static margin		4.1% M.A.C.
Aspect ratio	AR	1.5

Data on ascent vehicle:

Length	30 ft.
Diameter	5 ft.

The following formulae were used in determining the weights:

$$L = C_L \frac{1}{2} \rho \, S \, V^2 \tag{7a}$$

$$MR = \frac{1}{(\epsilon - \lambda_{PL}) + \lambda_{PL}} \tag{8a}$$

$$\epsilon = \frac{W_S}{W_i} \tag{9a}$$

$$\lambda_{PL} = \frac{W_{PL}}{W} \tag{10a}$$

For a detailed description of equipment weight see Appendix V.

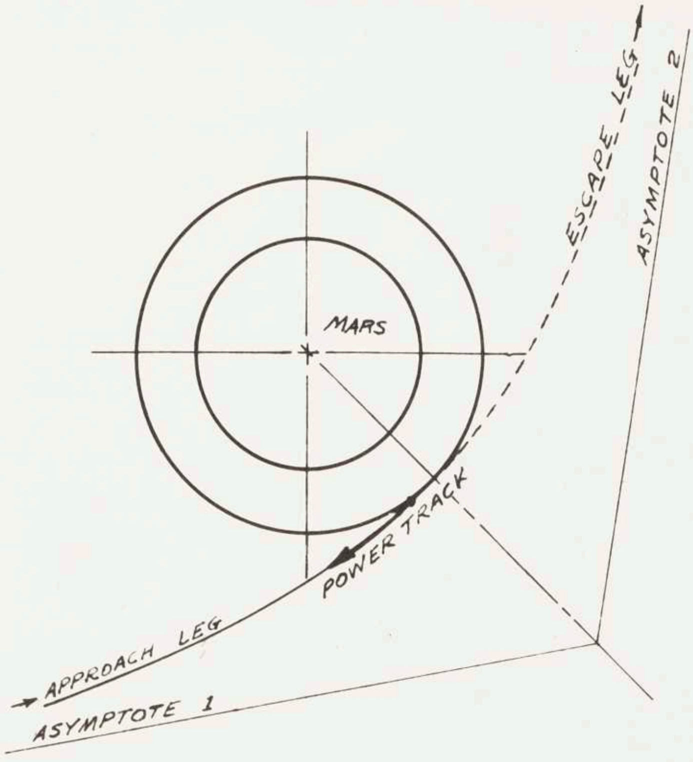
ESCAPE LEG
ASYMPTOTE 2
MARS
POWER TRACK
APPROACH LEG
ASYMPTOTE 1

FIG. 1a

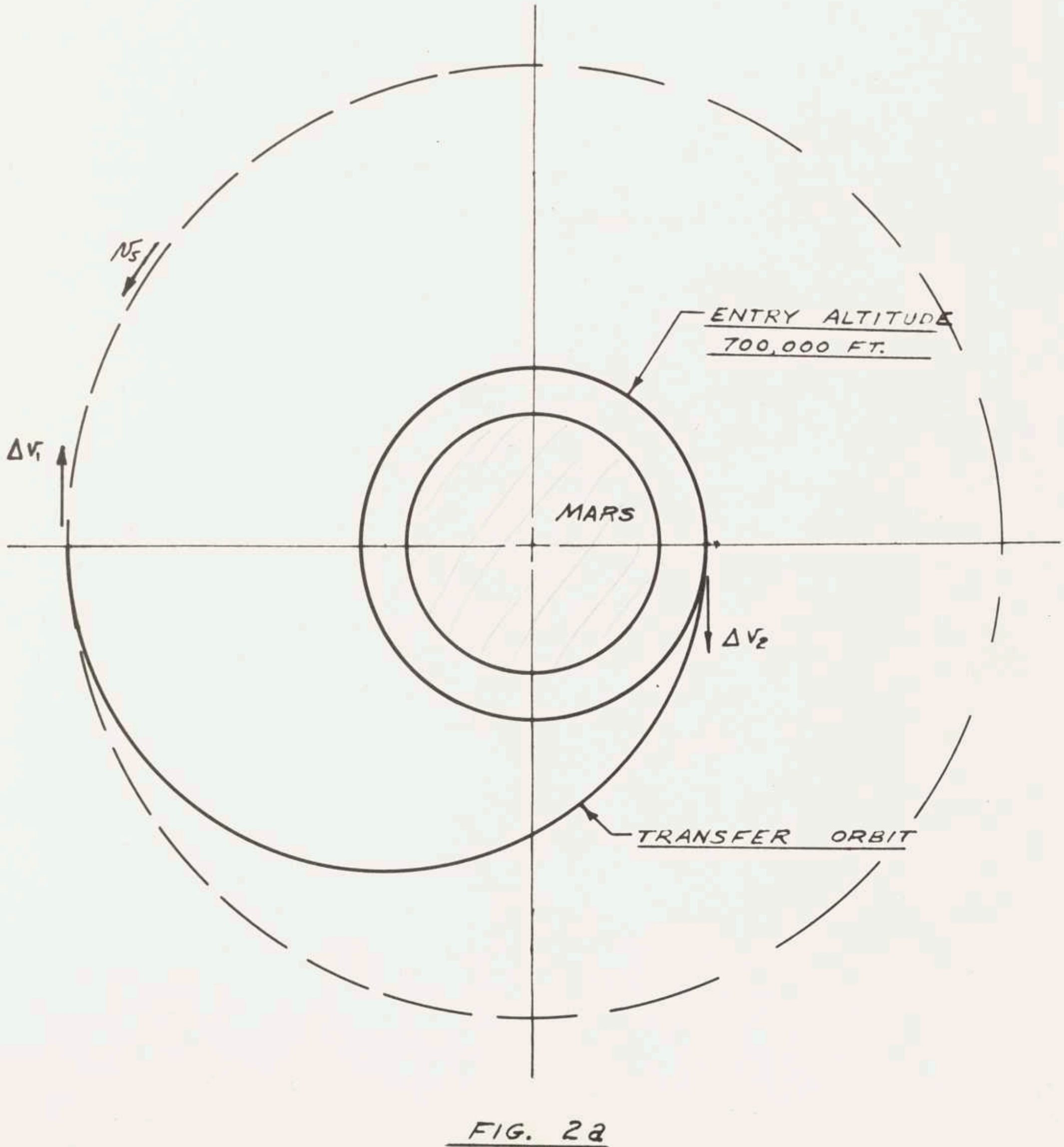
V_S
ENTRY ALTITUDE
700,000 FT.
ΔV_1
MARS
ΔV_2
TRANSFER ORBIT

FIG. 2a

CHAPTER II

DESCENT THROUGH THE ATMOSPHERE

SYMBOLS:

A	aspect ratio, b^2/s
C_L	lift coefficient
C_D	drag coefficient
C_{L_α}	$\partial C / \partial \alpha$
C_m	moment coefficient
$C_{m_{\dot\alpha}}$	rate of change C_m with rate of change of $\left\{ \frac{\dot\alpha l}{U}\left(\frac{\partial C_m}{\partial \dot\alpha l/V}\right)_{\dot\alpha \to} \right.$ (α PARAMETER)
C_m	rate of change C_m with pitching velocity parameter $\frac{\dot\theta l}{V}\left(\frac{\partial C_m}{\partial \dot\theta l/V}\right)_{\dot\theta \to 0}$
C.P.	center of pressure
D	drag
g	acceleration due to gravity
h	altitude above planet surface
l	reference length (mean aerodynamic chord)
m	mass (slugs)
q	dynamic pressure
r	distance from vehicle to center of planet
r_o	radius of Mars
R	leading edge radius or Gas Constant for Mars' atmosphere
s	distance along flight path
S	reference area (S_W)
S_T	elevon area
S_W	wing area including elevon area
t	time
T_{W_S}	stagnation point equilibrium maximum temperature
U	vertical velocity
$\bar{U}$	ratio of vehicle horizontal speed to circular orbital speed
V	horizontal velocity
W	weight at Earth's surface
X_T	distance from center of gravity to elevon C.P.
X_W	distance from center of gravity to wing C.P.
Z	dimensionless dependant variable defined by eq. 3b
Z'	$\partial z/\partial \bar{U}$

GREEK SYMBOLS:

α	angle of attack
β	atmospheric density decay parameter (ft^{-1})
γ	specific heat ratio
δ	control surface deflection (positive is down)
ϵ	surface emissivity
ϕ	descent angle measured from horizontal
ρ	air density
$\bar{\rho}_0$	surface air density that best fits a curve of log vs. h
σ	vehicle radius of gyration
Ω	vehicle velocity in flight direction.

SUBSCRIPTS:

i	initial
T	refers to elevons
w	refers to wing

Note: δ in fromt of a velocity or an angle indicates an incremental change of that quantity (in High Speed Glide Analysis)

DESCENT THROUGH THE MARTIAN ATMOSPHERE

The purpose of this section is to determine structural requirements, configuration requirements and performance. The descent will be considered in three phases: (I) hypersonic entry, (II) high speed glide, and (III) subsonic landing. The high altitude regime of free molecule flow will not be considered as causing different aerodynamic characteristics from the hypersonic continuum flow region since the maximum heat flow and maximum deceleration occur well outside the free molecule flow region according to Chapman. (Ref. 38).

PHASE I: HYPERSONIC ENTRY.

The entry will be defined as beginning at an altitude of 700,000 ft. The entering vehicle will have a velocity of 13,030 ft/sec in a direction tangent to the surface of Mars. At this altitude the speed for circular orbit is 11,460 ft/sec. Writing $F = ma$ in the vertical and horizontal directions we have the following equations of motion:

$$-\frac{d^2h}{dt^2} = \frac{dv}{dt} = g - \frac{V^2}{r} - \frac{L}{m}\cos\phi + \frac{D}{m}\sin\phi \qquad \text{(1b)}$$

$$\frac{dv}{dt} + \frac{Uv}{r} = -\frac{D}{m}\left(\cos\phi + \frac{L}{D}\sin\phi\right) \qquad \text{(2b)}$$

(See Fig. 1-a)

The following analysis is based on the method of Chapman (Ref. 38): in which these assumptions are made:

The term $\frac{UV}{r}$ can be neglected.

The altitude-density relation is: $\rho = \bar{\rho}_o e^{-\beta h}$

Lift and drag coefficients are constant.

In order to solve the equations of motion Chapman defines a new dimensionless dependant variable:

$$Z \equiv \frac{\bar{\rho}_o}{2\left(\frac{m}{C_D S}\right)} \sqrt{\frac{h}{\beta}}\, \bar{U} e^{-\beta h} \tag{3b}$$

With this substitution, Chapman has solved the equations and plotted the results for various entry initial conditions.

The maximum deceleration is: $g\sqrt{\beta r}\, \bar{U} Z_{max} \sqrt{1+\left(\frac{L}{D}\right)^2}$ (4b)

Since the vehicle is not a good heat sink we will determine the equilibrium skin temperature at the stagnation point when heat flow in equals radiation heat flow out, without accounting for heat absorbed. (Ref. 1) This reference indicates that the temperature aft of the stagnation point will be somewhat lower than at the stagnation point. The upper wing surface and the ascent vehicle will be shielded from the airstream and from the heat flow.

For Mars, the equilibrium skin temperature is given by:

$$T_{ws} = \frac{(.55)\, 3840 \left(\frac{W}{C_D S}\right)^{1/8} \bar{q}_\delta}{\epsilon^{1/4} R^{1/8}} \tag{5b}$$

From Ref. 33:

0.11	aluminum
0.80	steel
1.00	black body

METHOD OF ENTRY

It would appear desirable to use gasdynamic drag to reduce the speed of the vehicle to circular orbit velocity since the cost of shipping retro-rockets to accomplish this task would be very high. An entry at $L/D = 0$ was considered ($\bar{U}_i$ is 1.14). The results gave a maximum decelaration of 1.4 earth g's and a maximum stagnation temperature of 3800° R. This was considered too hot for our vehicle.

Chapman's results indicate that the temperature result cannot be lowered much. A positive L/D in the braking process will increase the temperature while a negative L/D will decrease it only slightly. This difficulty seems to be due to our large $\left(\frac{W}{C_D S}\right)$ ratio. Therefore, it was decided that, atmospheric braking is impractical for this vehicle and it will be necessary to use retro-rockets to reduce the entry speed to circular orbit velocity.

The results of two possible entry L/D ratios with entry speed equal to circular orbit velocity are presented below:

$L/D = 2.21$	ϕ_i	Max. deceleration (Earth g's)
$\alpha = 25°$	0°	0.35
$C_D = 0.21$	2.1°	0.37
$\frac{W}{C_D S} = 113$	4.3°	0.475

$T_{ws_{MAX}} = 1620°$ F. (T_{ws} does not vary much with ϕ)

$L/D = 1.5$	ϕ	Max. deceleration (Earth g's)
$\alpha = 34°$	0°	0.38
$C_D = 0.35$	2.1°	0.38
$\frac{W}{C_D S} = 66.7$	4.3°	0.43
$T_{ws_{max}} = 1560° F.$	6.4°	0.57

Lower values of L/D result in higher maximum accelerations and a high angle of attack that is awkward to control. Higher L/D will increase the maximum stagnation point skin temperature. It is evident from the above results that both L/D and entry angle may be varied considerably without excessive temperatures or accelerations resulting from this method of entry. The entry with $L/D = 2.21$ will be used as it will be easier to control.

LIFT AND DRAG COEFFICIENTS

The lift and drag during the entry were assumed to be given by Newton's equation with the constant term changed from 2 to 2.4 so as to agree with Shapiro's results for $M = \infty$. (Ref. 21)

$$C_L = 2.4 \sin^2\alpha \cos\alpha \tag{6b}$$

$$C_D = 2.4 \sin^3\alpha \tag{7b}$$

$$\alpha = \cot^{-1}\frac{L}{D} \tag{8a}$$

The speed of sound on Mars is:

$$a = \sqrt{\gamma R T} = 965 \text{ FT/SEC}$$

Shapiro gives the following equation for hypersonic flow:

$$\frac{C_L}{\alpha^2} = \frac{C_D}{\alpha^3} = \frac{\gamma+1}{2} + \sqrt{\left(\frac{\gamma+1}{2}\right)^2 + \frac{4}{(m\alpha)^2}} + \left[1-\left(1-\frac{\gamma-1}{2}M_\alpha\right)^{\frac{2\gamma}{\gamma-1}}\right] \qquad (9b)$$

at M = 3.5:

$$C_L = 3.2\,\alpha^2 \qquad C_D = 3.2\,\alpha^3$$

This shows that C_L and C_D are 1.33 times the Newtonian value at M = 3.5. Therefore at this Mach Number the total acceleration will be 1.33 times the value given by Chapman's analysis. However, this acceleration is still well below the structural requirements of 1.5 Earth g's.

CONTROL SURFACE DEFLECTION IN HYPERSONIC ENTRY

We will solve for the control surface area, S , by summing moments about the C.G. with $\alpha = 25^\circ$.

$$2.4 \sin^2\alpha\, S_W X_W q = 2.4 \sin^2(\alpha+\delta)\, S_T X_T + 2.4 \sin^2\alpha\, A_T X_T q \qquad (10b)$$

for:
- S_W = 800 sq. ft.
- X_W = 1.25 ft. (static margin: 4.06%)
- X_T = 15.70 ft.
- S_T = 64 sq. ft.

Aileron (Elevon) dimensions: b = 8 ft.
c = 4 ft.

RANGE OF THE HYPERSONIC PHASE

The hypersonic phase will be considered to have ended when the leading edges of the wing become subsonic. This occurs at a Mach Number of M = 3.5 (τ = 0.295).

Chapman gives the following for the range:

For Mars: $$\frac{\Delta s}{r} = \frac{1}{14.1}\int_{\bar{U}_2}^{\bar{U}_1} \frac{d\bar{U}}{Z} \qquad \text{(11b)}$$

This equation was solved by plotting a graph of $\frac{1}{Z}$ vs. $\bar{U}$ and graphically integrating the area. The result is:

$$\frac{\Delta s}{r} = 3.1$$

This surprising result was checked by a more approximate relation given by Glazely.

$$\frac{\Delta s}{r} = \frac{1}{2}\frac{L}{D} \ln \frac{1}{2}\beta r\left[1-(\bar{U})^2\right] = 4.8 \qquad \text{(12b)}$$

Therefore it can be seen that we have the right order of magnitude. The first answer is probably more accurate and it will be used hereafter.

ALTITUDE FOR WHICH M = 3.5

Using the assumed altitude-density relation of $\rho = \bar{\rho}_o e^{-\beta h}$ we can solve for the altitude by use of Chapman's Z-function.

$$e^{-\beta h} = \frac{2}{\bar{\rho}_o}\sqrt{\frac{\beta}{r}}\left(\frac{m}{C_D S}\right)\frac{Z}{\bar{U}} \qquad \text{(13b)}$$

for $\bar{U}$ = 0.295 $\qquad h$ = 262,000 ft.

PHASE II: HIGH SPEED GLIDE

To begin Phase II, the pilot will nose down to maximum L/D so as to extend the period of the glide in order to have sufficient time to choose a suitable landing spot.

If we neglect surface curvature and satellite velocity effects the linearized equations of motion in body axes are:

$$m\left[\left(\frac{d\Omega}{dt}\right)_i + \frac{d\delta\Omega}{dt}\right] = -S_w C_D\left[q_i + \delta q\right] - mg\left[\phi_i + \delta\phi\right] \tag{14b}$$

$$m\Omega_i \frac{d\delta\phi}{dt} = S_w C_L\left[q_i + \delta q\right] - mg \tag{15b}$$

The steady-state solution to these equations is:

$$\phi_i = \frac{D/L}{1 + \frac{\beta\Omega_i^2}{2g}} \tag{16b}$$

$$\left(\frac{d\Omega}{dt}\right)_i = \frac{1}{2}\Omega_i^2 \beta \phi_i \tag{17b}$$

Love in Ref. 46 experimentally determines L/D ratios for various delta wings over a considerable speed range. His experiments on a wing of similar aspect ratio, thickness ratio, and section , indicate that we can expect an average maximum L/D of 4 at $\alpha = 6^{\circ}$. (This includes an allowance for parasite drag of the vertical surfaces and the ascent vehicle). The values of L/D do not change very much from when the wing first became subsonic (in our case M = 3. 5) to lower subsonic speeds.

With this value of L/D we can solve equations 16 b and 17b in a stepwise manner by determining new values of ϕ_i and Ω_i for eacc step. The results are tabulated below:

	Ω_i FT/SEC	ϕ_i RAD	$t-t_1$ SEC	$\left(\frac{d\Omega}{dt}\right)_i$ FT/SEC	h_i FT
1	3380	0. 027	0	2. 67	262, 000
2	2000	0. 067	440	2. 2	245, 000
3	1000	0. 147	590	1. 2	156, 000
4	500	0. 214	625	0. 3	76, 000

With the slopes and the altitude changes we can estimate the range of this phase. Range, Phase II $=$ 970 nautical miles.

PHASE III: LANDING

Jones shows in reference 44 that the lift curve slope of a low aspect ratio delta wing is $\frac{\pi S}{2}$. He shows experimentally that this value of C_{L_α} is true subsonic and supersonic as long as the Mach cone lies well ahead of the leading edge.

For our wing $C_{L_{\alpha_W}} = 0.260$

$$\frac{L_{total}}{q} = (S_W - S_T)\, C_{L_{\alpha_W}} + \text{cross flow lift on elevon} + \text{trim force due to } \delta$$

$$\frac{L}{q} = (S_W - S_T)\, C_{L_{\alpha_W}} \alpha + S_T C_{L_{\alpha_W}} (\alpha + \delta) - S_T C_{L_\delta} \delta \quad \text{(18a)}$$

For balance, the moments about the C.G. $= 0 =$

$$S_W X_W C_{L_{\alpha_W}} \alpha - S_T X_T C_{L_{\alpha_W}} \alpha + S_T X_T C_{L_{\alpha_W}} (\alpha + \delta) - S_T X_T C_{L_\delta} \quad \text{(19b)}$$

The last terms of equation 18b require closer inspection. With the elevons hinged about a point 1.2 ft. behind its leading edge; and with a gap between the leading edge of the elevon and the trailing edge of the wing, the air can flow over the top of the elevon when it is at a negative (up deflection). The force on this surface is estimated to be the sum of the cross-flow force and the force due to the deflection from $\delta = 0$. The C_{L_δ} was assumed to be 5. See Fig. 13-C for clarification of this.

With these estimations equations 18b and 19b have been solved to give:

When $\alpha = 24^{o}$

$\delta = -9.5^{o}$

$C_L = 0.90$

LANDING SPEED

$$L = W = \frac{1}{2}\rho U^2 A_w C_L$$

$\rho = 0.00023$ (Ref. 25)

$U = 287$ ft/sec $= 169$ knots

LONGITUDINAL DYNAMIC STABILITY DURING ENTRY:

During the entry the possibility exists for several modes of oscillation. Chapman shows that a slow phugoid will result from a non-zero entry angle. (See Fig. 2b) This mode, by itself, does not seem to give serious trouble as long as the entry angles are small (See previous results of various entries). However, Tobak (Ref. 48 & 94) shows the existance of a considerably faster and sometimes divergent longitudinal mode. Qualitatively, this mode seems to be caused by the changing of the aerodynamic "spring force." As the vehicle enters, the "spring" (the lift which acts through a center behind the center of mass) is stiffened by the increasing dynamic pressure. However, as the drag increases a point may be reached where dynamic pressure is decreasing with time. Then the "spring" is becoming less stiff with time and the angle of attack oscillations will diverge if the damping is insufficient. Ref. 48 gives the following condition for convergence:

$$-\beta \lambda_3 \rho(h) - \frac{1}{4} \frac{\frac{\partial q}{\partial \phi}}{q(h)} > 0 \tag{20b}$$

WHERE:

$$\lambda_3 = \frac{S}{4 \beta m \sin \phi} \left[-C_{L_\alpha} + \left(\frac{l}{\sigma} \right)^2 \left(C_{m_q} + C_{m_{\dot\alpha}} \right) \right] \tag{21b}$$

We will evaluate this relation at an altitude where divergence seems likely. At an altitude of 262,000 ft., the deceleration is a maximum so that $\frac{\partial q}{\partial \phi}$ may be near its most negative value.

For: h = 262,000 ft. $\quad \Omega$ = 3380 ft/sec $\quad \alpha$ = 25°

Ref. 93 gives values for $C_{m_q} + C_{m_{\dot\alpha}} \approx -0.40$

$$C_{L_\alpha} = \frac{\partial C_L}{\partial \alpha} = \frac{\partial (3.2\alpha^2)}{\partial \alpha} = 6.4\,\alpha = 2.8$$

σ = 11.5 ft.

Chapman gives the path angle:

$$\phi = \frac{Z' - Z/\bar{u}}{\sqrt{\beta r}} = 0.0462 \text{ radians} \tag{22b}$$

$$\rho = 0.0125\,\rho_0 = 2.9 \times 10^{-6} \text{ slugs/cu. ft.}$$

$$-\beta \lambda_3 \rho = 0.535 \times 10^{-4}$$

This low value of damping seems largely due to the very low density.

We will next evaluate: $\frac{1}{4} \frac{\frac{\partial q}{\partial \phi}}{q}$

Chapman gives:

$$q = \sqrt{\beta r}\, Z\, \bar{u}\, \frac{W}{C_D S} \tag{23b}$$

q = 46.5 lbs/sq. ft. at h = 262,000 ft.

By using Chapman's graph of 30 $\bar{U}$ Z vs. $\bar{U}$ (Fig. 2b) and the above relations it was possible to evaluate Z, q, and ϕ for various values of U and thus determine Z' and $\frac{\partial q}{\partial \phi}$.

$$\frac{-\frac{1}{4}\frac{\partial q}{\partial \phi}}{q} = +0.224$$

The inequality (20a) is not satisfied and the angle of attack oscillations will diverge. At the very low density it appears unlikely that the aerodynamic damping can be made sufficiently large to prevent divergence. We will therefore determine the period of the oscillation to see if it is slow enough to be controlled.

Ref. 48 gives:

$$\omega = \sqrt{\frac{\beta C_L S K_z'}{2m}}\ \Omega(\phi)\sqrt{\rho(\phi)} \qquad (24b)$$

where:

$$K_z = \frac{-C_{m_\alpha}}{C_L \beta \ell}\left(\frac{\ell}{\sigma}\right)^2 \qquad (25b)$$

0.73 rad/sec

The period is 8.6 seconds. It would seem that this oscillation is slow enough to be controlled.

DISCUSSION OF GASDYNAMIC EFFECTS ON CONFIGURATION:

It was desired to reduce center of pressure travel to a mini mum in order to maintain static stability and control throughout the flight regime. A symmetrical section delta wing seems to fulfill this requirement as the C.P. stays very nearly at the two-thirds root chord position throughout the various flight regions. Ref. 46 experimentally confirms this; however, it indicates that there may be a slight forward travel of the C.P. at low speeds. In spite of the probability of this slight C.P. travel it was decided to make the static margin 4.1% so as to help control and to reduce the loss of lift due to control deflection at landing. This static margin should be large enough to preserve static stability throughout the C.P. range. In order to further improve the effectiveness of the elevons at low speeds, they are hinged about a point 1.2 ft. behind their leading edges and a gap was placed between the leading edge of the elevon and the trailing edge of the wing so as to encourage flow over the top of the elevon when it is at a negative (up) deflection. To improve elevon effectiveness at hypersonic speeds the trailing edge was squared off. The purpose of the blunted leading edges is to reduce the maximum skin temperature. The vertical fin area was chosen so as to reduce the chances of Phillips Roll instability (Ref. 69) by making the natural frequencies in pitch and yaw nearly equal.

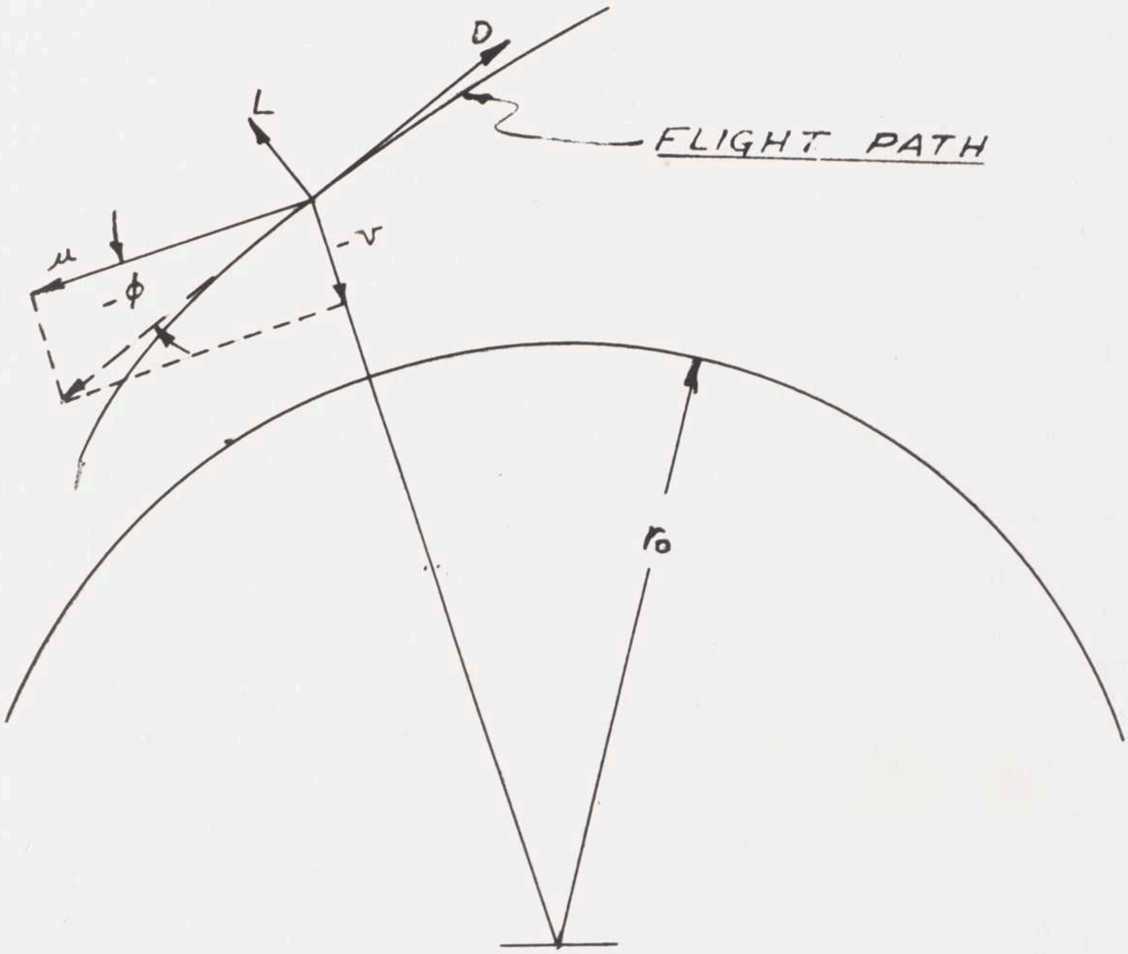

SYMBOLS AND COÖRDINATES FOR ENTRY

FIG. 1b

FIG. 2b

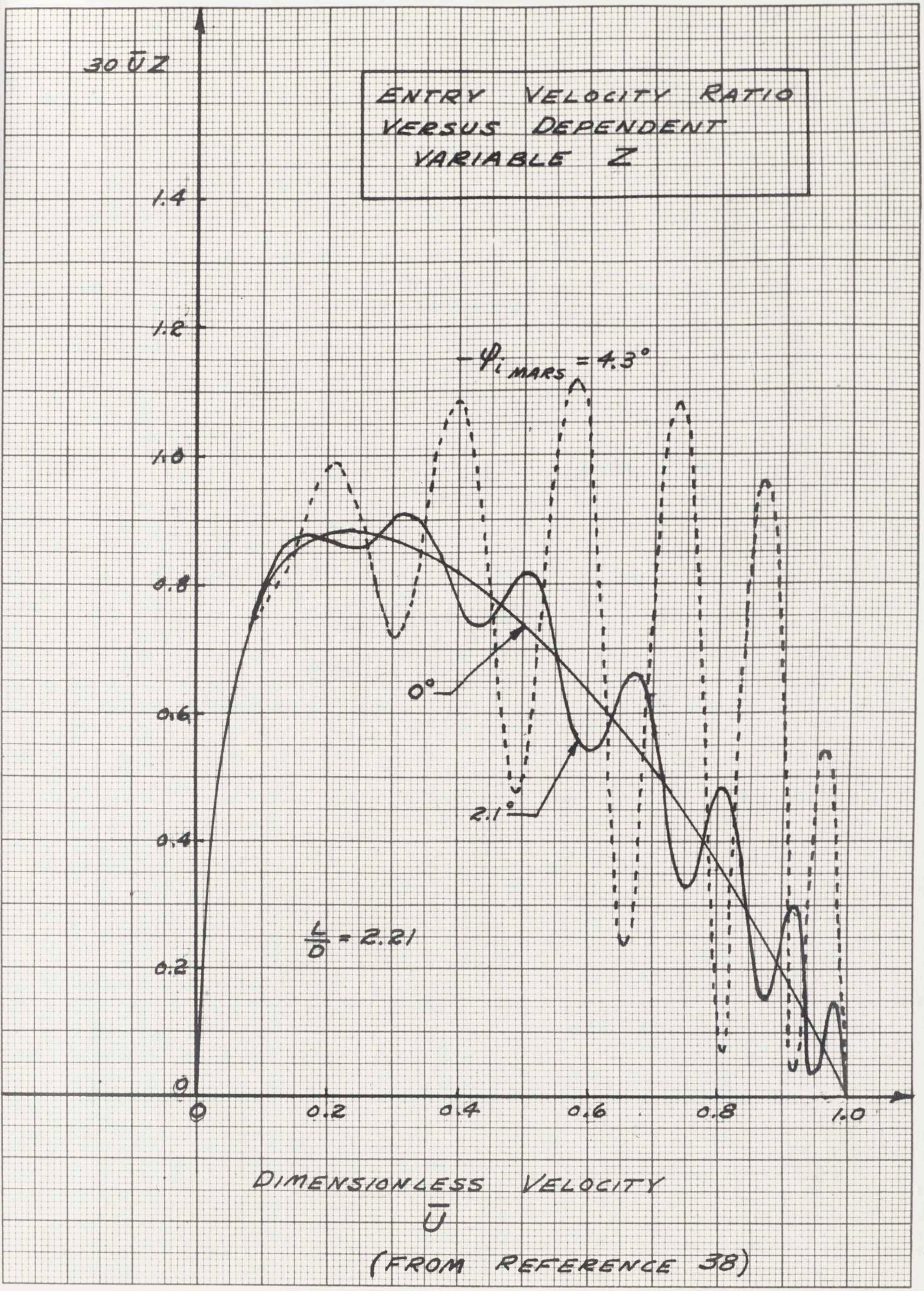

30 $\bar{U}$ Z
ENTRY VELOCITY RATIO VERSUS DEPENDENT VARIABLE Z
1.4
1.2
1.0
0.8
0.6
0.4
0.2
0
$-\varphi_{i_{MARS}} = 4.3°$
0°
2.1°
$\frac{L}{D} = 2.21$
0.2
0.4
0.6
0.8
1.0
DIMENSIONLESS VELOCITY
$\bar{U}$
(FROM REFERENCE 38)

CHAPTER IV

STRUCTURAL DESIGN

SYMBOLS:

A	total stringer area
b	wing thickness, ft.
E	modulus of elasticity
F_c	average compressive stress
L	length
M	moment
$R(x)$	1/2 chord thickness, f(x)
t	thickness of metal sheet
w	effective width
y	distance from neutral axis to outermost fiber in beam
X_{ss}	static stability margin, ft.

GREEK SYMBOLS:

σ	tension or compression stress, psi
σ_{MA}	maximum allowable stress
τ	shear stress

STRUCTURAL DESIGN OF ASCENT VEHICLE

The structural design problem is to determine a structure that is capable of withstanding the loads in various environmental condition, and will also remain within the weight allowance.

During entry the ascent vehicle will have to withstand a lateral load of about 0.5 earth g's. However, this load may be considerably higher if the entry angle is much greater than 0°. The temperature environment in this phase is not severe as the ascent vehicle is shielded by the wing which is at an angle of attack of 25°. Since the maximum heating occurs early in the entry phase where the flow does not contact the ascent vehicle, it appears reasonable to use aluminum construction. This material is particularly attractive when one considers the high cost per pound of transferring the vehicle to a circum-Martian orbit.

The landing loads are uncertain because nobody knows what the surface will be like. The absolute minimum landing lateral load would be 0.39 earth g's. In order to allow for this uncertainty and the uncertainty of the entry load factor, the ascent vehicle will be designed to withstand a lateral load of 1.5 earth g's.

During ascent the vehicle must be able to withstand an axial load of 3.5 earth g's, which occurs during final adaptation to the satellite orbit.

Structural design is of prime importance in a design of this type. It is literally worth spending millions of dollars to get the structural weight reduced by a few pounds. The savings in fuel weight for the entire mission makes this possible. A considerable percentage of the cost of developing the vehicle would go into cutting structural weight to a minimum. This design represents what we think is a reasonable preliminary design figure for the weight.

I. PRIMARY LOADS ON ASCENT VEHICLE.

The loads are due to three sources; payload, structure, and fuel. The payload consists of the pilot and navigator with their respective equipment. Assume the load to be divided into two primary groups and their c. g. placed at either end of the crew compartment. The structure is assumed to be evenly distributed along the entire vehicle length, except for the rocket engine and nozzle, which is a concentrated load.

II. ASCENT VEHICLE SUPPORT BRACKETS.

The front support is logically placed at the junction of the nose and the cylindrical body proper. The rear support is more complicated because the only support points available are at either end of the fuel tank. A freely pivoted cantilever beam carries the resultant load to an intermediate point arbitrarily placed at 22.6 feet from the nose of the vehicle.

III. WEIGHT AND BALANCE CALCULATION.

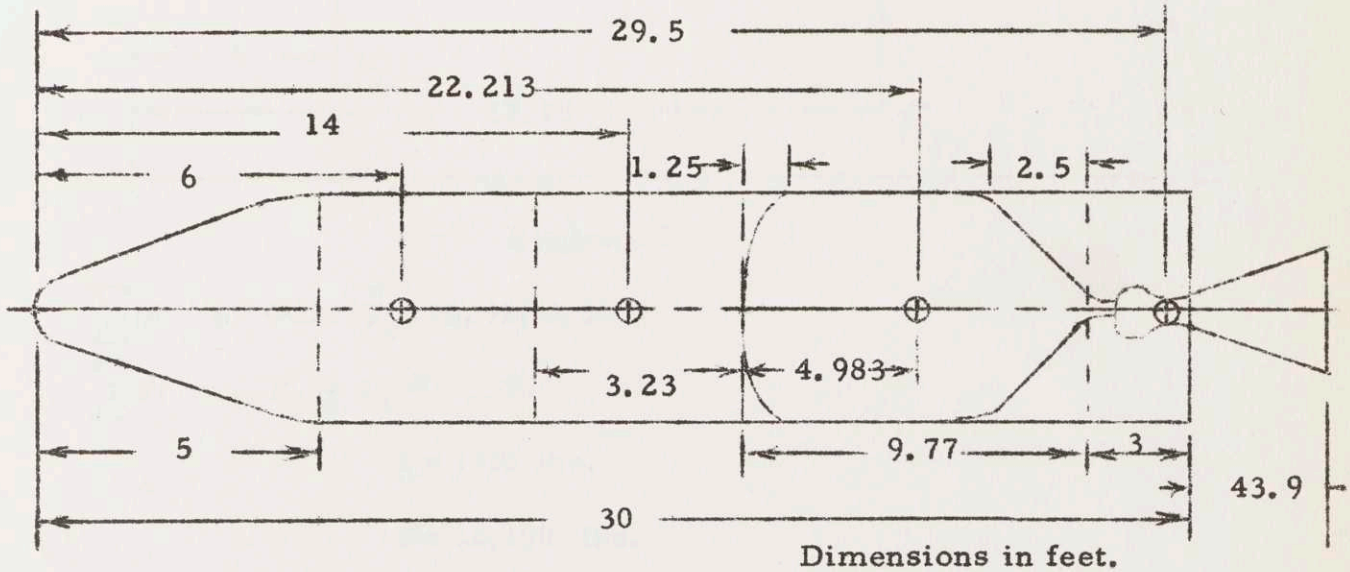

Diagram 1.

Transverse Loads for Entry at 1.5 Earth G's.

Weights:	W_i = 13,500 lb.	Distributed Load, Ws
	W_{PL} = 700 lb.	42.333 lb/ft at 1 g
	W_S = 1,345 lb.	63.5 lb/ft at 1.5 g
	W_P = 11,455 lb.	

Weight and Balance:

	W	x	M_x	1.5W
1. Pilot and Equipment	350	6.0	2100	525 lb.
2. Navigator and Equipment	350	14.0	4900	525
3. Fuel	11,455	22.213	254500	17183
4. Engine	75	29.5	2183	112.5
5. Structure	1270	15	19050	1905
$\Sigma W =$	13,500		282,688	

$$C.G. = \frac{Mx}{W} = 20,92$$

Now that the C.G. is known, the reaction forces at the vehicle supports can be calculated assuming a rear pivot point position of 22.6 feet from the nose.

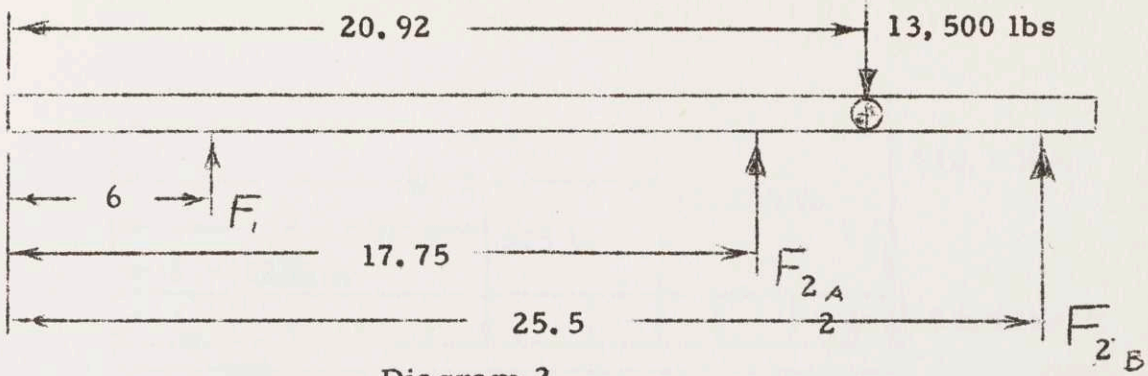

Diagram 2.

$\sum M$: $6F_1 + 22.6F_2 = 20.92(13,500)$

$\sum F$: $F_1 + F_2 = 13,500$

$F = 1310$ lbs.

$F = 12,190$ lbs.

Rear Support Arm.

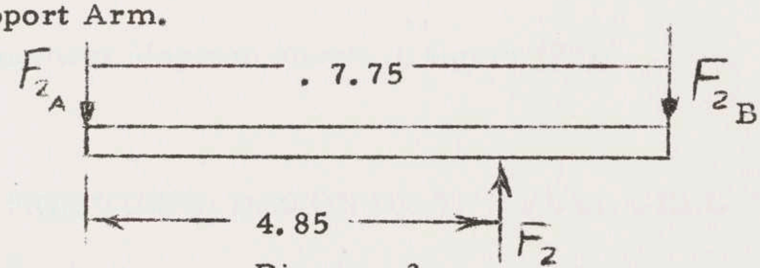

Diagram 3.

$\sum M$: $(4.85)(12,190) = F_{2_B}(7.75)$

$F_{2_B} = 7640$ lbs.

$F_{2_A} = 4550$ lbs.

Values for 1.5 g:

$F_1 = 1965$ lbs.

$F_{2_A} = 6820$ lbs.

$F_{2_B} = 11460$ lbs.

Shear and Moment Calculation.

The total loading on the vehicle for the 1.5 g transverse loading condition is shown by diagram (4).

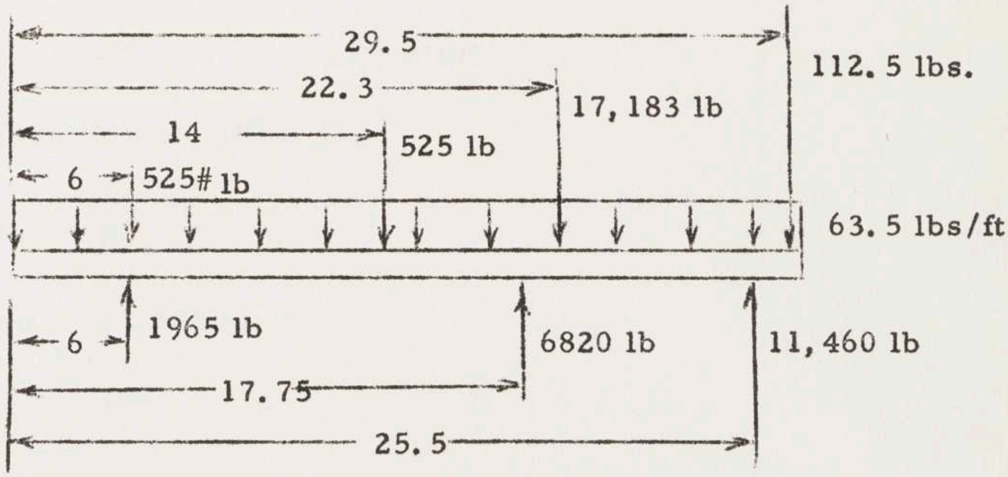

Dimensions if feet.

Diagram 4.

This loading produces the shear diagram shown in Figure (lc) and the moment diagram shown in figure (2c).

STRUCTURAL DESIGN OF THE FUEL CELL

The section area moment of inertia for a thin walled cylinder is derived below.

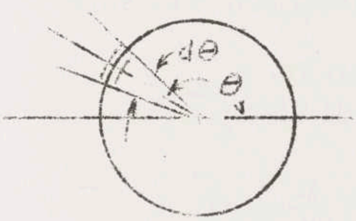

$$I = AR^2$$

$$I = \int_0^{2\pi} (R\,d\theta\,t)(R^2 \sin^2\theta)$$

Diagram 5.

$$I = 2\pi R^3 t \ \ \mathrm{in}^4 \qquad \text{(lc)}$$

For the fuel cell: $t = 0.05$ in. $R = 30$ in.

then $I = 8480 \ \mathrm{in}^4$

1. CALCULATION OF THE STRESSES DUE TO TRANSVERSE LOADING

Bending Stress (Ref. 14)

$$\sigma = \frac{My}{I} \tag{2c}$$

$M_{max} = 34,200$ lb-ft
$y = 2.5$ ft.
$\sigma = \pm 1455$psi

Shear Stress due to Bending (Ref. 14)

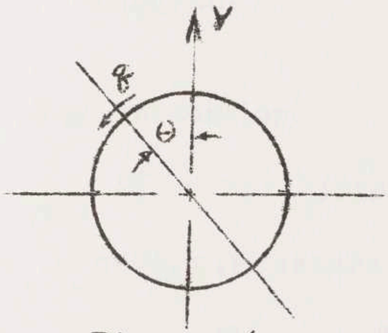

Diagram 6.

$$q = \frac{V}{I}\int y\, dA \tag{3c}$$

Integrating for a circular ring:

$$q = \frac{V}{\pi R} \sin\theta \tag{4c}$$

value is a maximum at $\theta = 90^\circ$.

$V_{max} = -11,040$ lbs.
$q = 117$ lb/in

$\tau = \frac{q}{b}$ where b is thickness of the sheet

$\tau_s = 2334$, $\theta = 90^\circ$.

2. CALCULATION OF STRESS DUE TO INTERNAL LOADING

σ_L = Axial tension due to end pressure,

σ_H = circumferential tension.

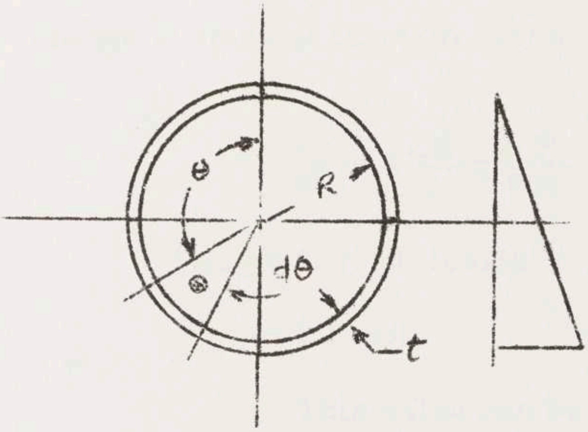

$$P_o = \frac{P_{max}}{2}$$

Diagram 7.

For end tension:

$$\sigma_L = \text{Force}_L/\text{area of skin stress} \tag{6c}$$

$$\text{Force}_L = (\text{Pressure at center of } \Delta A)\Delta A \tag{7c}$$

$$P = \frac{P_{max}}{2} - \frac{2}{3}\frac{P_o}{2}\cos\theta \tag{8c}$$

$$= 2.605 - 1.736 \cos\theta \text{ psi}$$

$$\sigma_L = \frac{PR}{2t} \tag{9c}$$

$$\sigma_L = 782 \quad 521 \cos\theta$$

For hoop stress:

$$P = 2.605(1-\cos\theta) \tag{10c}$$

$$\sigma_H = \frac{PR}{t} \tag{11c}$$

$$\sigma_H = 1565(1-\cos\theta) \text{ psi}$$

Shear stress due to change in hoop stress with vertical distance..

The loading varies from a minimum at the top of the fuel cell to a maximum at the bottom. The variation in the forces tangential to the surface of the skin produces a shear flow in the skin

$$q_{ave} = \frac{\Delta P}{L} = \frac{\Delta P}{\pi R} \tag{12c}$$

$q_{ave} = 0.0553$ lbs/in

$\tau_H = 1.1$ psi (from eq. 5c)

This value can be neglected in comparison to the bending stress.

Tabulation of Stresses in Fuel Cell. See Diagram 8.

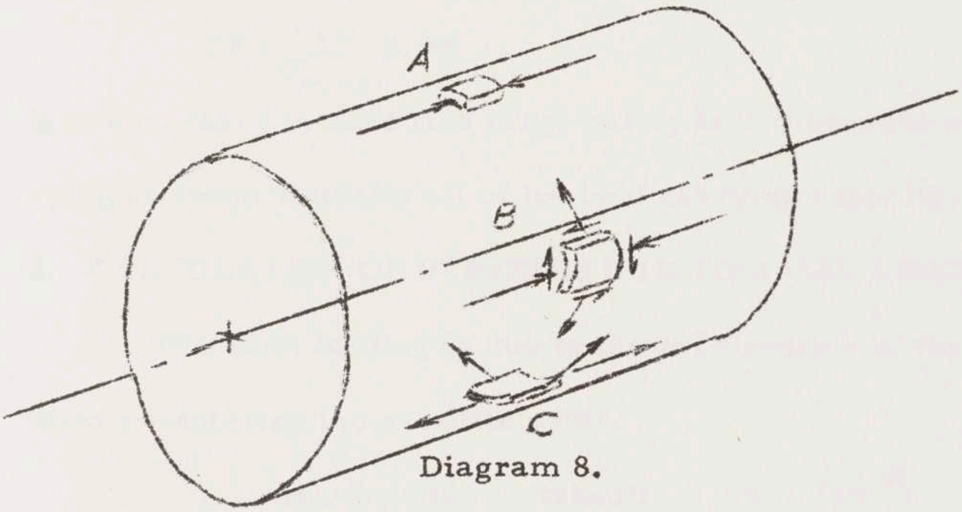

Diagram 8.

	A	B	C
	psi	psi	psi
σ_B	-1455	0	1455
σ_L	261	782	1303
σ_H	0	1565	3130
τ	0	2334	0

Perform a Mohr's circle analysis on each elemental area.

Summation of maximum stress in fuel cell

	A	B	C
	psi	psi	psi
$\sigma_{MAX.\,TEN.}$	0	3511	3130
$\sigma_{MAX.\,COMP.}$	-1194	-1161	0
τ_{MAX}	0	2336	0

3. CRITICAL BUCKLING STRESS

The buckling stress in a cylindrical shell is given in Ref. 19 by the empirical equation:

$$\frac{\sigma_{CR}}{E} = 9\left(\frac{t}{R}\right)^{1.6} + 0.16\left(\frac{t}{L}\right)^{1.3} \tag{13c}$$

$$= 3.54 \times 10^{-4}$$

$$\sigma_{CR} = 3680 \text{ psi}$$

The safety factor is:

$$SF = \frac{\sigma_{CR}}{\sigma_{MAX}} = 3.08 \tag{14c}$$

It is necessary to have this large safety factor because a buckled cylinder loses virtually all of its load carrying capacity.

4. CALCULATION OF STRESSES DUE TO AXIAL LOADING.

The axial loading is due to the acceleration of the vehicle when re-entering the satellite orbit.

Acceleration: takeoff 2.64 ft/sec^2

burn-out 103.6 ft/sec^2

Acceleration of gravity 12.55 ft/sec^2

At launch, the inertial loading is added to the gravitational loading because the acceleration is normal to the surface of the planet.

The end of the first power phase sees the track tangential to the surface with the velocity of the vehicle equal to the same order of magnitude as orbital velocity.

Maximum acceleration occurs at the burnout of the second power phase, the adaption maneuver. When at near orbital velocity, there is no gravitational loading on the vehicle.

Absolute acceleration:

Take-off - 15.18 ft/sec^2

Burn-out - 103.6 ft/sec^2

The greatest axial load occurs at the bottom of the fuel cell, or at Section A; see Diagram 9.

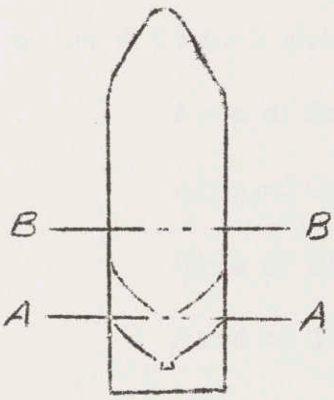

Diagram 9.

Fuel weight = total weight minus weight of fuel in the supporting cone volume 9836 lbs.

$$\text{Structure Mass} = \frac{L_A}{L_T} M = 35.1 \text{ slugs}$$

Tabulation of Loadings due to Axial Acceleration

	Mass	Loading Take-off	Burn-out
Payload	21.7	329	2245
Structure	34.1	517	5350
Fuel	305	4630	0
Total		5476	7595

For take-off acceleration:

σ_{COMP} = loading/cross-sectional area of cylinder

= 581 psi

$\sigma_H = \frac{PR}{t}$ 834 psi

$\sigma_L = 0$

For burn-out acceleration:

$\sigma_{COMP} = 805$

$\sigma_H = 0$

$\sigma_L = 0$

5. WEIGHT CALCULATIONS

The weight calculations for the fuel cell are based upon the area of the 0.05 inch sheet as shown in the construction in Figure 10c.

Area of dome	2870 in^2
Area of Cylinder	13560
Area of Cones	3770
Area of Tube	189
Total Area	20,389

For t = 0.05 inches, Volume = 1020 in^3 additional volume

Additional volume for support rings and welds is 500 in^3.

Total Volume 1500 in^3.

Weight = ρV_T

= 152 lbs.

STRUCTURAL DESIGN OF THE FORWARD BODY

The maximum shear and moment which acts on the forward body section is obtained from Figure 1c and Figure 2c.

$$M_{max} = 5300 \text{ ft-lbs}$$

$$V_{max} = 1059 \text{ lbs.}$$

1. CALCULATION OF STRESSES DUE TO TRANSVERSE LOADING.

BENDING STRESS

$$q = \frac{U}{\pi R} \sin\theta = 10.1 \text{ lbs/in}$$

$$\tau = \frac{q}{B} = 202 \text{ psi}$$

STRESS DUE TO CABIN PRESSURIZATION

$$P = 8 \text{ psi}$$

$$\sigma_L = \frac{PR}{2t} = 2400 \text{ psi}$$

$$\sigma_H = \frac{PR}{t} = 4800 \text{ psi}$$

Tabulation of Stress. See Diagram 8.

	A	B	C
	psi	psi	psi
σ_B	-750	0	750
σ_L	2400	2400	2400
σ_H	4800	4800	4800
τ_o	0	202	0

From Mohr's Circle diagram:

$$\sigma_{MAX} = 4800 \text{ psi}$$

$$\tau_{MAX} = 1200 \text{ psi}$$

Forces are all in tension and there is no possibility of compressive buckling.

2. CALCULATION OF STRESSES DUE TO AXIAL LOADS.

From Diagram 9, the load acts at section B.

Structure mass = 24.0 slugs.

Loading due to acceleration:

	Mass	Take-off	Burn-out
Payload	21.7	329.0	2245
Structure	24.0	364.0	2485

The Compressive stress:

σ_{COMP} = 234 psi critical for burnout.

The safety factor is

SF = 15.6

3. CONSTRUCTION OF CENTER SECTION.

Using unreinforced construction with 0.05 inch thick skin, the forward body is stable as there are no compressive stresses. However, to facilitate the attachment of the cabin components, a series of annular rings of channel section is proposed as support for the loads, see Figure (10c).

The channel section has a large flange on the skin side which reduces the shear and moment transfer to the skin and minimizes the local bending deflections of the skin.

Provision must be made for the airlock, which will introduce local skin stiffeners and a door mechanism. Physiological limitations seem to indicate a separate compartment in the rear of the forward body occupying half of the cross-sectional area. The opposing half can be used for storage.

The tentative internal component arrangement suggests the pilot's chair be fully forward and the navigator's chair be as far to the rear as possible limited by the airlock construction.

4. WEIGHT CALCULATIONS.

The distribution of components are as shown in Figure (10c).

Weight of skin	128 lbs.
Weight of stringers	20 lbs.
Weight, Total	148 lbs.

5. DESIGN OF THE NOSE CONE.

The nose cone has a clear fused silica plate window (Ref. 35), on the upper surface bonded to the aluminum sheet by an aluminum molding which is attached to its circumference.

Weight calculation based upon distribution of components shown in figure (10c).

Weight of skin	35.8 lbs
Weight of nose molding	44
Weight of silica plate	34.7
Weight of aluminum molding	11 lbs.
Total weight	125.5 lbs

IV. OTHER CONSIDERATIONS.

The remainder of the allotment of structural weight, $w \cong 900$ lbs, is distributed among the different components of the guidance and propulsion system; the rocket thrust mount, the gimbal cage, the forward body installations, the reinforcement for the air lock, the inertial navigation system with its ascent trajectory computor, the gimbal mount actuators, and the many sensing devices on the control panel. Provisions must also be made for a wing-ascent vehicle control tie-in.

For the crew cabin design, the change in attitude of the vehicle necessitates a multi-position chair that can be oriented so that the accelerations are normal to the body axis. During the stay on the planet the chairs must extend into sleeping cots.

STRUCTURAL DESIGN OF THE WING

The function of the wing is to carry the ascent vehicle from the circum-Martian orbit to the surface without creating excessive loads. The given quantities about which the wing is designed are:

Wing area $800\ ft^2$

Aspect ratio 1.5

Total load 18000 lbs.

I. WEIGHT AND BALANCE CALCULATION.

All values for position are measured from the leading edge of the chord. The center of pressure, for a delta-wing, lies at $\frac{2}{3}$ chord and remains constant over the angle of attack range.

For stability, the static-stability margin is 0.041 of the mean aerodynamic chord

$$X_{ss} = 1.25 \text{ feet.}$$

The C. G. position lies at

$$X_{cg} = X_{cp} - X_{ss}$$

$$X_{cg} = 29.55 \text{ feet}$$

The total configuration is arranged so that the C. G. of the ascent vehicle falls at this point. This means that the wing alone has a C. G. at this point. If the C. G. of the wing structure happens to fall on any other point, the payload weight can be adjusted to give the required C. G.

II. THE WING LOADING, SHEAR, AND MOMENT CONSIDERATIONS.

Assume that for the flight range the pressure distribution is proportional to the wing area distribution as depicted by the kinetic theory of lift distribution. The operational extremes that the structure has to withstand are 1.5 g at entry from orbit and .39 g static landing loads. The critical condition is the 1.5 g acceleration at entry.

1. Loading Diagram.

All loads are based upon 1/2 of the wing area as the quantities are symmetrical about the center line.

$$\text{Total load} = 1.5(W_g/2) = 13{,}500\text{lbs.}$$

$$\text{Semi-span} = b_{w/2} = 17.3 \text{ ft.}$$

$$\text{Average distributed load} = 780 \text{ lbs/foot}$$

$$\text{Linear distributed load} = 90.1\,X$$

where X is the distance from the tip t o the chord section.

The values of loading, shear, and moment versus span position from the center line are given in Figure 3c.

2. Chordwise Loading.

Choose the chord that lies closest to the ascent vehicle or 2.5 feet from the center line, see Diagram 10.

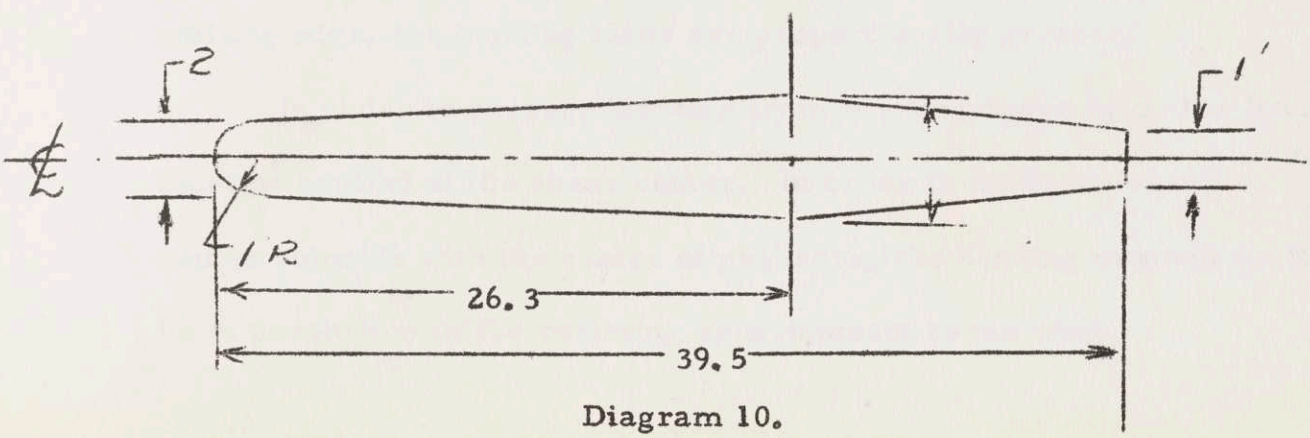

Diagram 10.

At this span position,

V = 9850 pbs (Fig 3c)

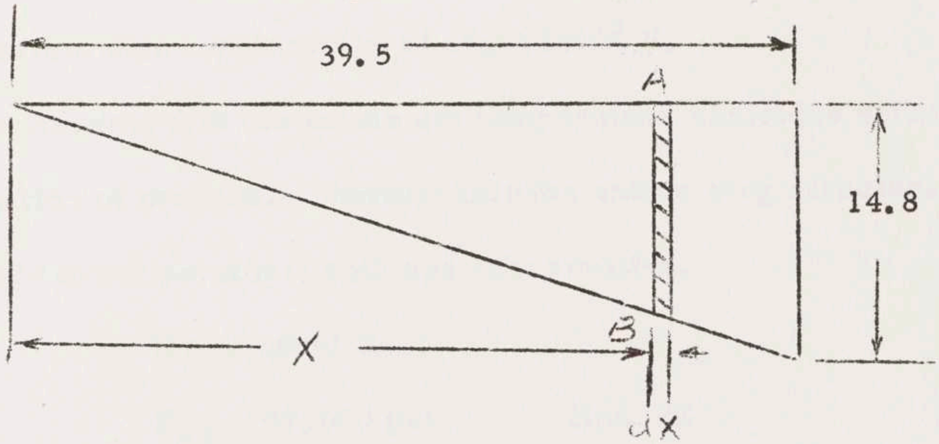

Diagram 11

P Load/Area 33.75 lbs/ft^2

Assume an elemental distance of unity: $dx = 1$. Then, at the base chord:

The Load	33.75 lbs/ft chord
The Shear	12.62X lbs/ft chord
Moment	$6.31X^2$

where X is defined in Diagram 11. These values are given in Fig. (4c).

III. STRINGER AREA AND DISTRIBUTION.

The bending loads in the wing are resisted by stringers placed along the surface of the wing. Because of the greater span at the trailing edge, the bending loads are proportionally greater.

In order to prevent the wing from twisting under load, the load must be applied at the shear center. In order to make the shear center coincide with the center of pressure, the bending moment must be in proportion to the resisting area moment of the wing.

1. Maximum Allowable Stress.

The temperature environment for the wing produces an equilibrium skin temperature of about 1400° F.

Assume that the maximum temperature coincides with the application of maximum load and that the entire wing structure reaches the highest temperature; both are conservative.

Use Inconel X:

F_{su}	47,000 psi	Ref. 22
F_{sy}	19,000 psi	Table 5-3
E	20×10^6	

Maximum allowable stress $= 85\%$ F_{su}.

$\sigma_{MA} = 39,900$ psi

use a safety factor of 1.1:

$\sigma_{MA} = 36,300$ psi

2. Stringer Area for span beams.

Area moment for stringers at the surface of the wing:

$$I = AR^2 \qquad \text{(1d)}$$

Substituting My/σ_{MA} for I, then

$$A = M/\sigma_{MA} R \qquad \text{(2d)}$$

$A = 2.76 \times 10^{-5}$ M/R area per ft chord.

The graph of jA versus chord position is shown in figure (5c).

Effective Widths.

The skin thickness has been chosen as 0.02 inches on the top and 0.012 on the bottom, from Ref. 14. The effective width is 1/2 the effective skin width over the stringer.

$$w = 0.85t\sqrt{E/F_c} \tag{3d}$$

$w = 0.4$ inches

Total effective length $= 0.8$ in.

Effective area $= 0.016$. in^2

For the top of the wing, which is in compression, the area effective in bending is the stringer area plus the effective skin area. At the bottom of the wing, all fibers are in tension and the entire skin is effective.

Assume that the stringer area on the bottom is large enough to attach the span shear webs.

$A = 0.04\ in^2$

Construct skin of sheet inconal with milled stringers.

Tabulation of Stringer Area

Station	Stringer Area on Top
6.5	0.054
15	0.044
19	0.074
23	0.108
26	0.064
28	0.084
30	o.112
32	0.151
34	0.203
35.5	0.117

36.5	0.138
37.5	0.166
38.5	0.200
39.5	0.116

Stringer area on bottom $= 0.04$ in.^{2}

3. Shear Web Thickness.

The span beams must carry shear loads as well as bending loads.

$$V_{max} = 1160 \text{ lbs at station } 23$$

Assuming that the critical stress is the buckling shear stress, then from Ref 14:

$$F_{s_{cr}} = KE\left(\frac{t}{b}\right)^2$$

where K is a function of a/b.

a the distance between chord webs = 4 feet

b height of span web.

To find the thinkness,

$$KE\left(\frac{t}{b}\right)^2 = 1.1\frac{V}{tI}(A)(R) \quad \text{where } I = AR^2$$

$$t^3 = 6.6 \times 10^{-7}\ U_b\ /\ K \qquad \text{at station 23, } t = .069 \text{ in.}$$

Assuming that the shear web buckles initially at about 45° to the shear load. For a pure tension field

$$\sigma_S = \sigma_T = \frac{V}{th} \qquad \text{Ref 14}$$

$$t = \frac{V}{\sigma_T h} = .000925 \text{ in.}$$

Actually, the shear web does not form a pure tension field because the web is not perfectly flexible and will resist the buckling loads. Shear webs resistant to buckling will support bending as well as shear loads. Practical webs can resist some diagonal shear stress after buckling and then act in an intermediate range between shear resistant webs and pure tension field webs.

Assume a thickness of 0.01 inches for the intermediate range.

4. Stringer area for Chord Beams.

M_{max} between station 6.5 and station 15

$M_{max} = 1220$

$A = 0.028 \text{ in}^2$

Net stringer area $= 0.012 \text{ in}^2$

5. Weight Calculations for the Wing.

Volume of material used:

Upper skin	0.995 ft^3
Skin stiffeners	0.304 ft^3
Lower skin	1.333 ft^3
Span stringers	0.672 ft^3
Spanshear webs	0.702 ft^3
Chord Stringers	0.010 ft^3
Chord shear webs	0.13 ft^3
Total Volume	4.146 ft^3
Weight	2140 lbs

The remainder of the structural weight allowance, about 550 pounds, is allotted to wing carry through structure, the landing gear unit (see figure (8c)), the ascent vehicle support structure (see figure (13c) , the ascent vehicle erection mechanism, and the vertical tail assembly.

The wing carry through structure sustains the shear loadings of the ascent vehicle body and carries the moments under the ascent vehicle from wing to wing. The details of this structure are shown in Figure (9c) and Figure (7c). It is possible that when the vehicle is erected the protrudence of the rocket nozzle will necessitate the removal of the rear brace to provide an unobstructed opening for the pivoting of the vehicle.

The landing gear is composed of a retractable front skid and two hydraulic extensible skids along the lower tail surfaces. These units are also manually operated to raise the wing platform high enough to swing the ascent vehicle to a vertical position. The rocket engine support structure rests upon a small tripod while the wing supports are removed.

The mechanism to raise the ascent vehicle is a pulley arrangement fastened to the tips of the upper tail surfaces.

The construction of the vertical tail is the same as that of the wing with carry through clips to the wing spar stringers.

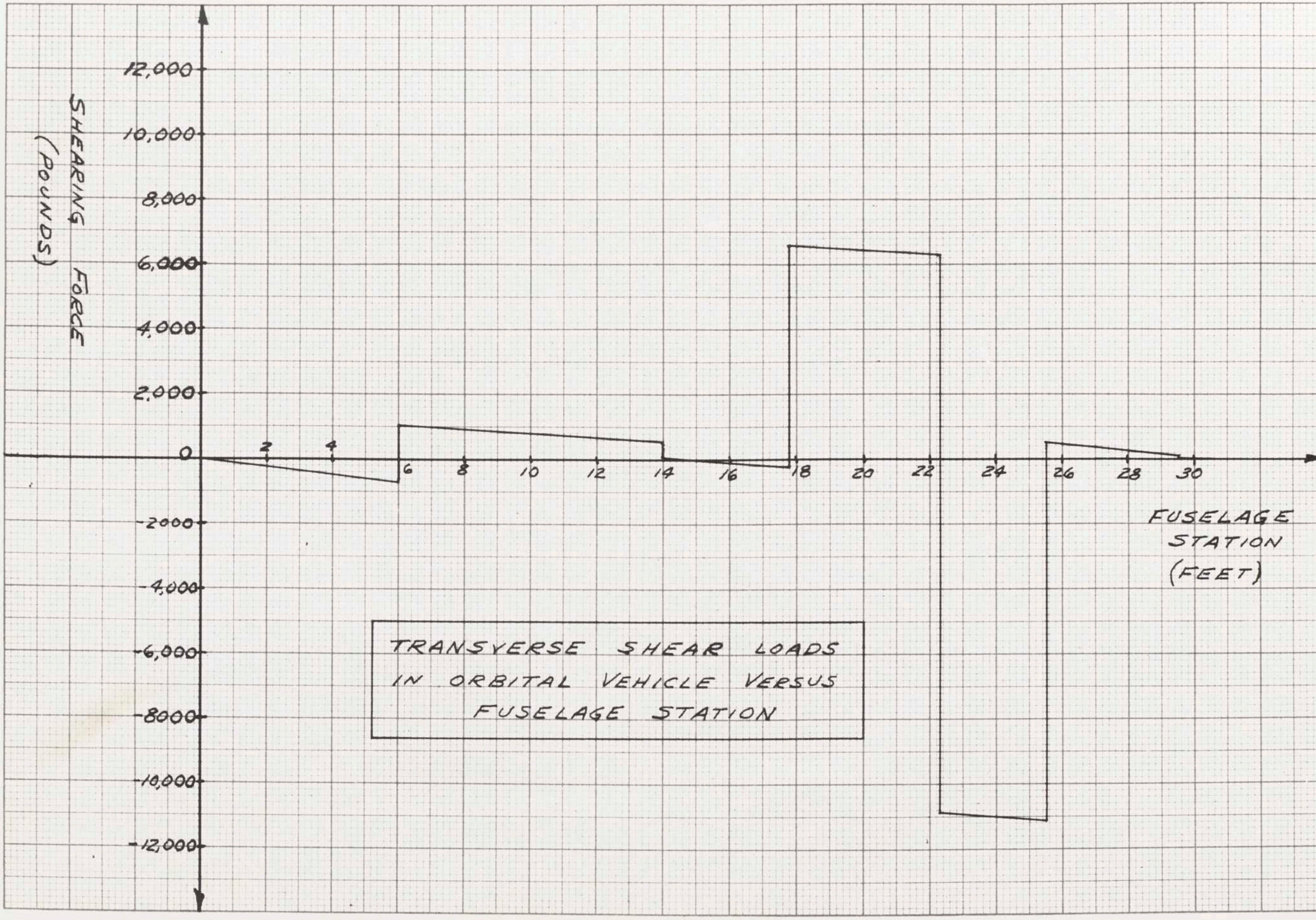
SHEARING FORCE (POUNDS)
12,000
10,000
8,000
6,000
4,000
2,000
0
-2000
-4,000
-6,000
-8000
-10,000
-12,000
2
4
6
8
10
12
14
16
18
20
22
24
26
28
30
FUSELAGE STATION (FEET)
TRANSVERSE SHEAR LOADS IN ORBITAL VEHICLE VERSUS FUSELAGE STATION

FIG. 1c

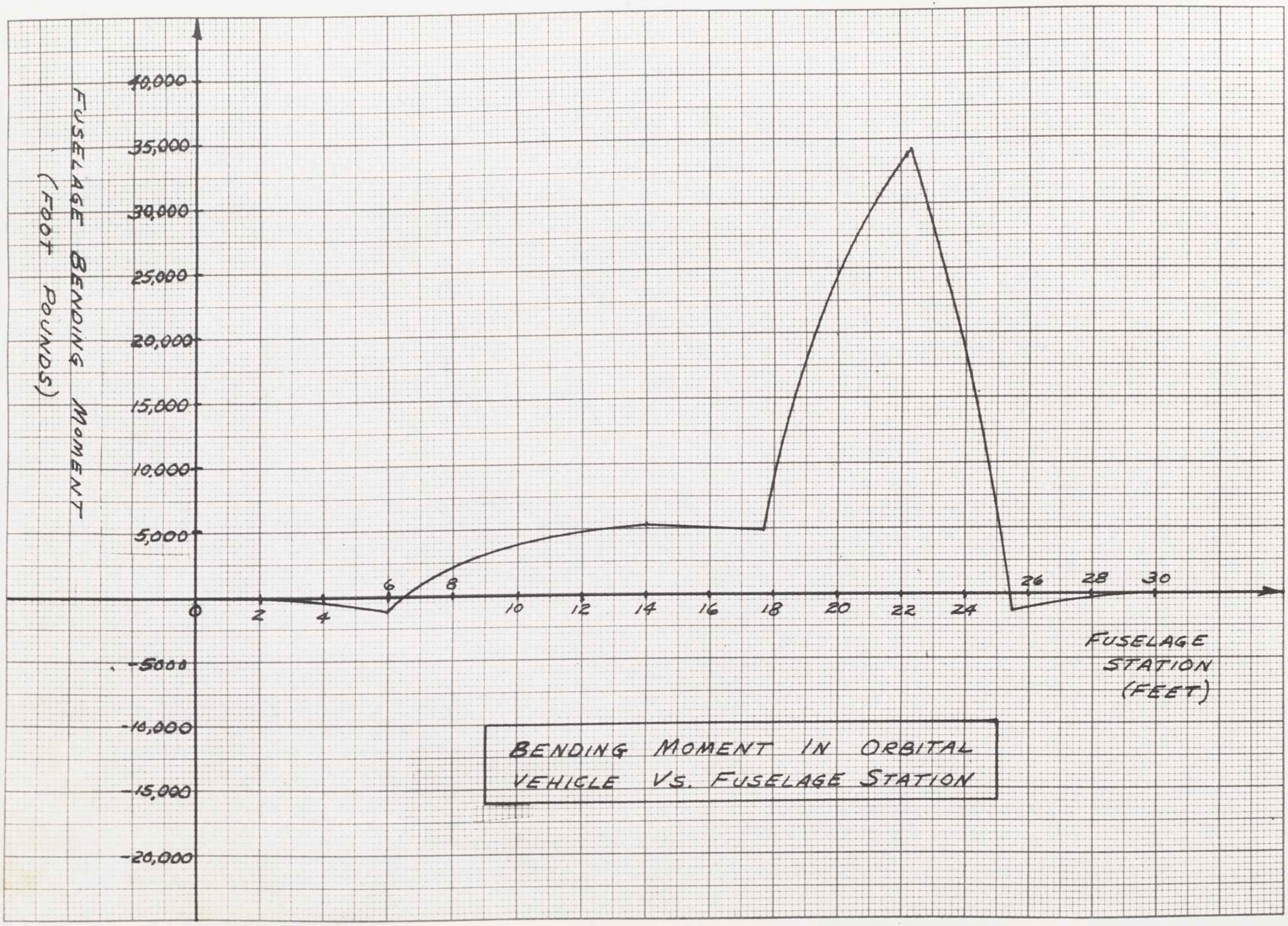

BENDING MOMENT IN ORBITAL VEHICLE VS. FUSELAGE STATION

FIG. 2c

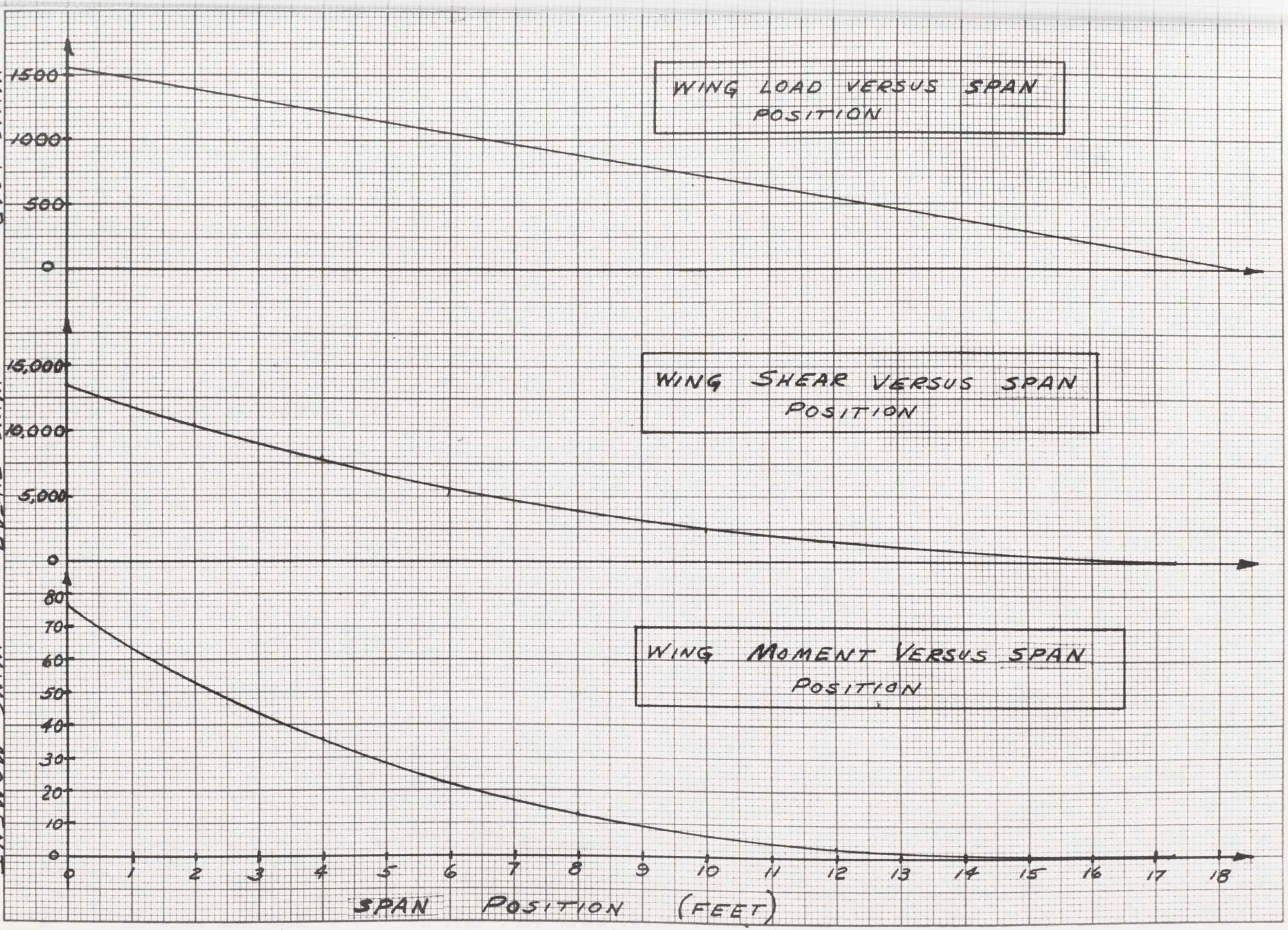
WING LOAD VERSUS SPAN POSITION
WING SHEAR VERSUS SPAN POSITION
WING MOMENT VERSUS SPAN POSITION
WING LOAD (POUNDS)
1500
1000
500
0
WING SHEAR (POUNDS / IN²)
15,000
10,000
5,000
0
WING MOMENT (FT LBS x 10⁻³)
80
70
60
50
40
30
20
10
0
0 1 2 3 4 5 6 7 8 9 10 11 12 13 14 15 16 17 18
SPAN POSITION (FEET)

FIG. 3C

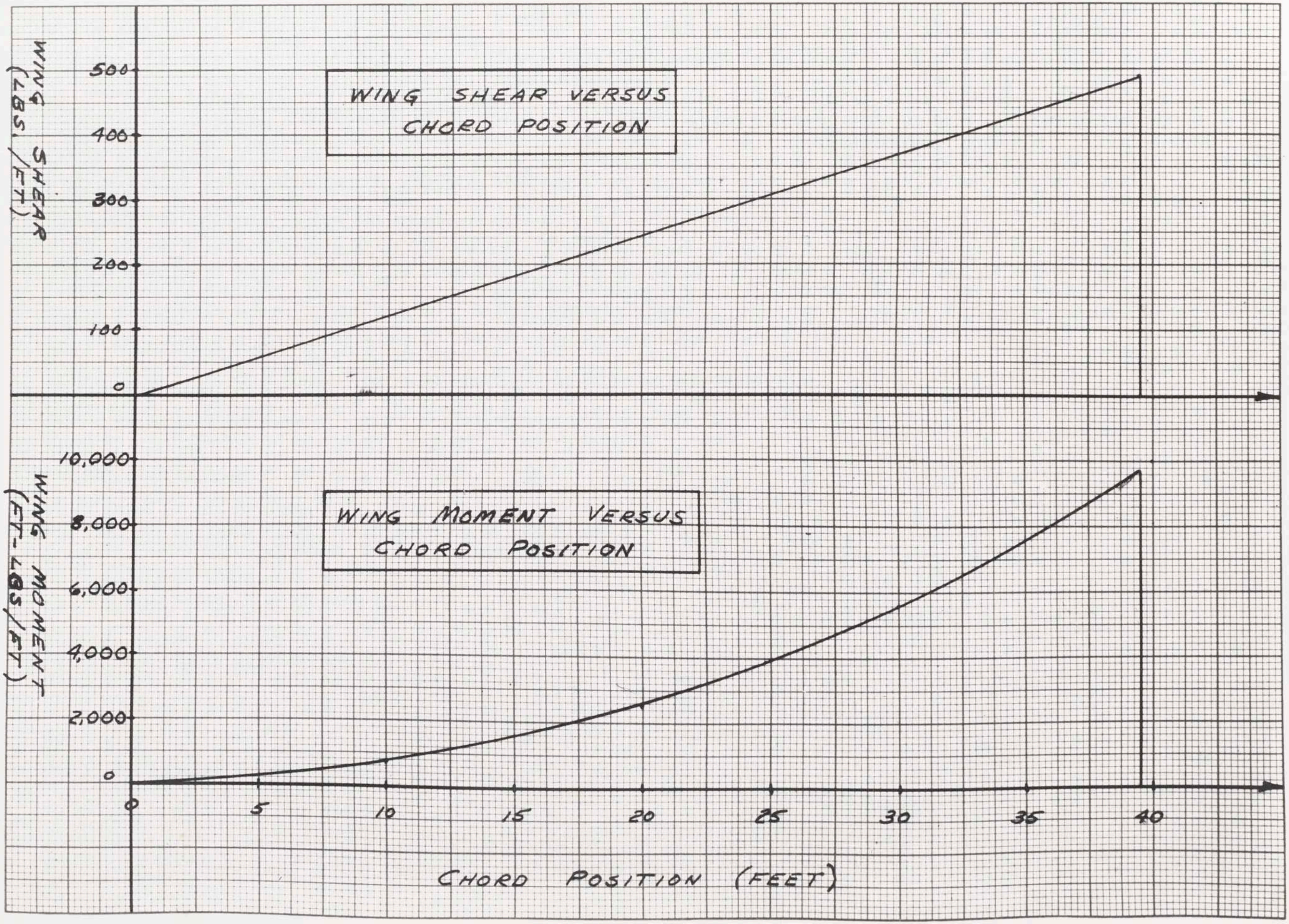
WING SHEAR VERSUS CHORD POSITION
WING SHEAR (LBS./FT.)
500
400
300
200
100
0
WING MOMENT VERSUS CHORD POSITION
WING MOMENT (FT-LBS/FT)
10,000
8,000
6,000
4,000
2,000
0
0
5
10
15
20
25
30
35
40
CHORD POSITION (FEET)

FIG. 4C

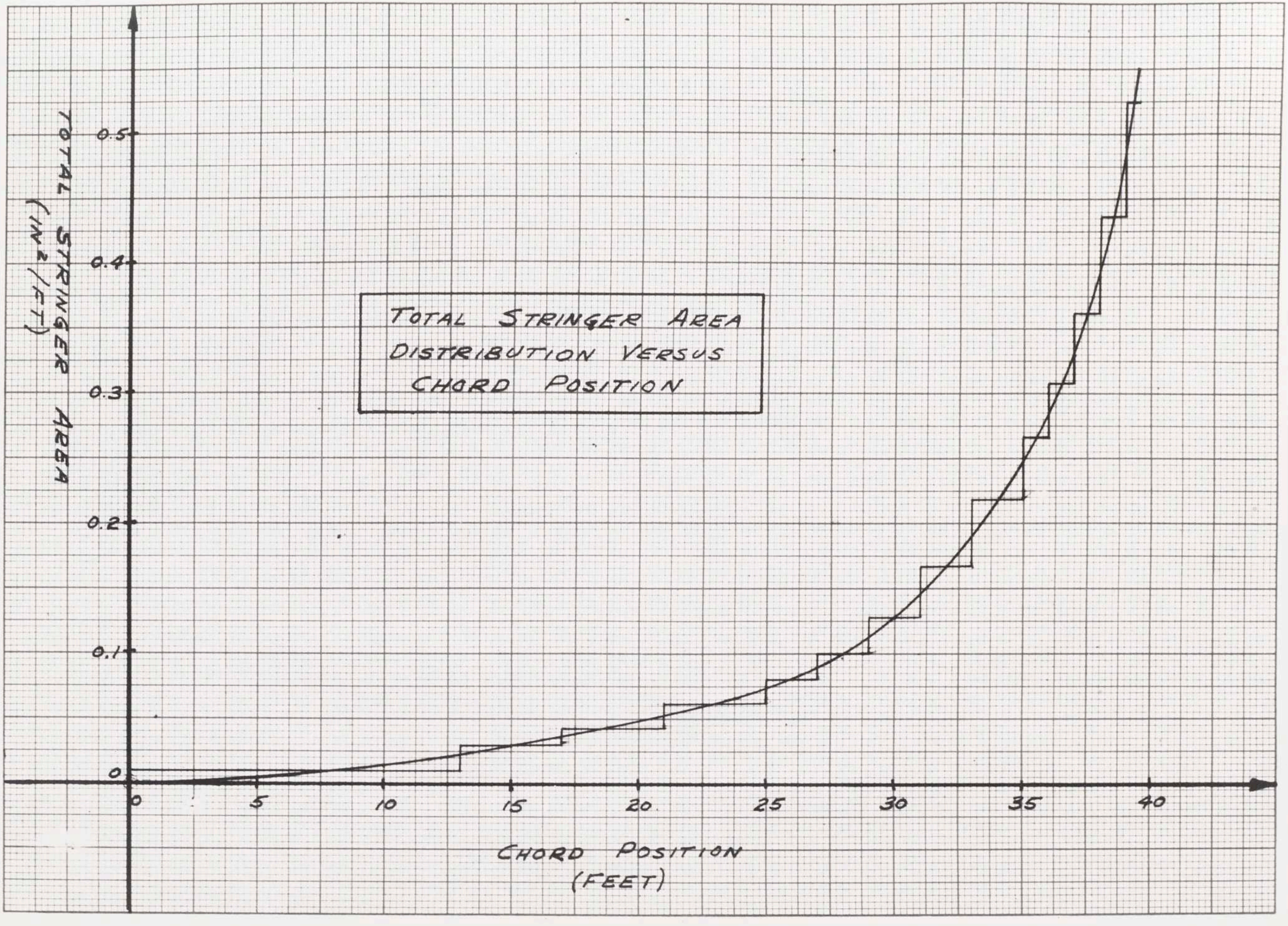
TOTAL STRINGER AREA
DISTRIBUTION VERSUS
CHORD POSITION
TOTAL STRINGER AREA
(IN²/FT)
0.5
0.4
0.3
0.2
0.1
0
0
5
10
15
20
25
30
35
40
CHORD POSITION
(FEET)

FIG. 5C

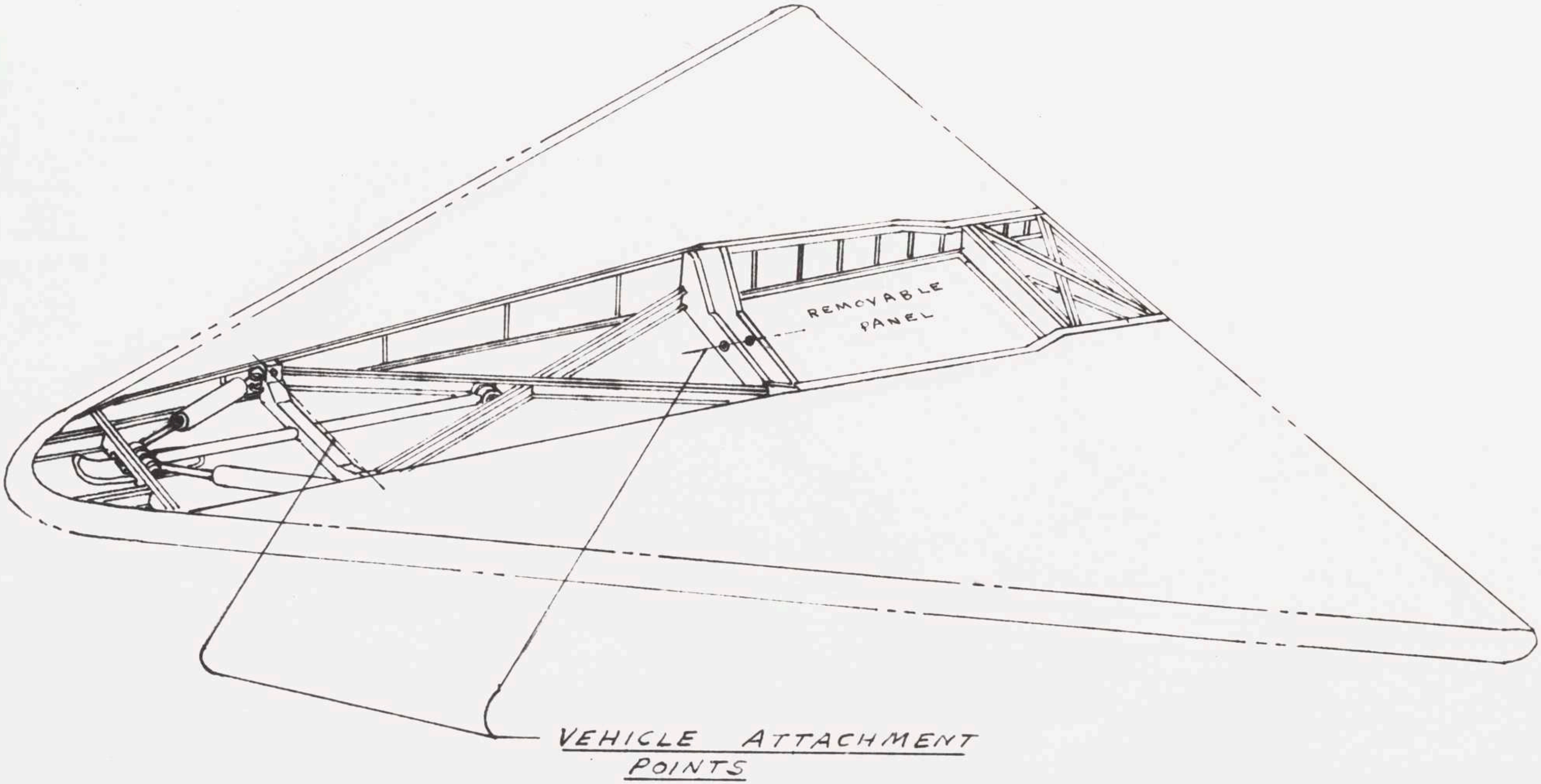

SKETCH OF WING CENTER SECTION
WITH LANDING GEAR
FOLDED & VEHICLE NOT
IN PLACE

FIG. 7c

19

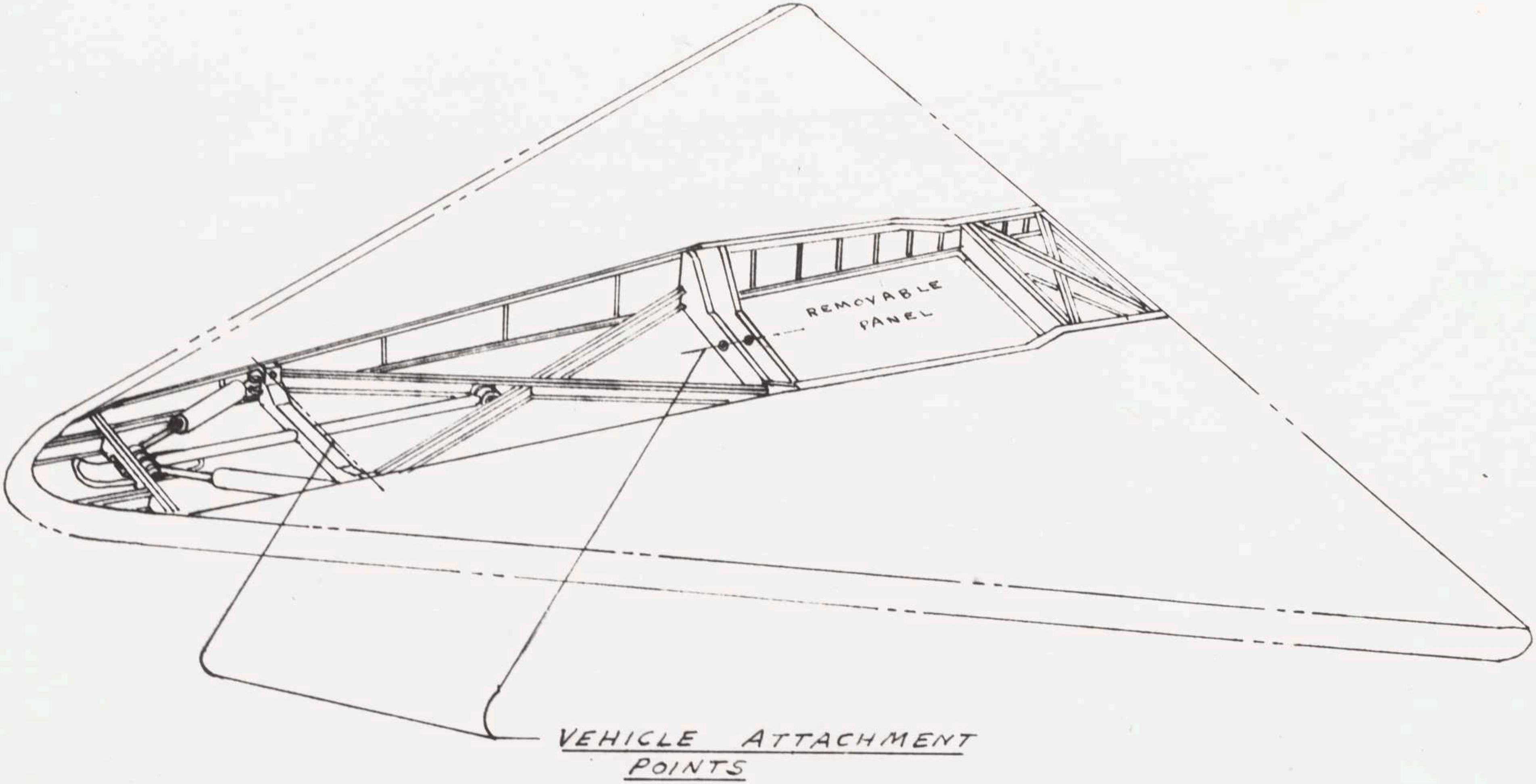

SKETCH OF WING CENTER SECTION
WITH LANDING GEAR
FOLDED & VEHICLE NOT
IN PLACE

FIG. 7C

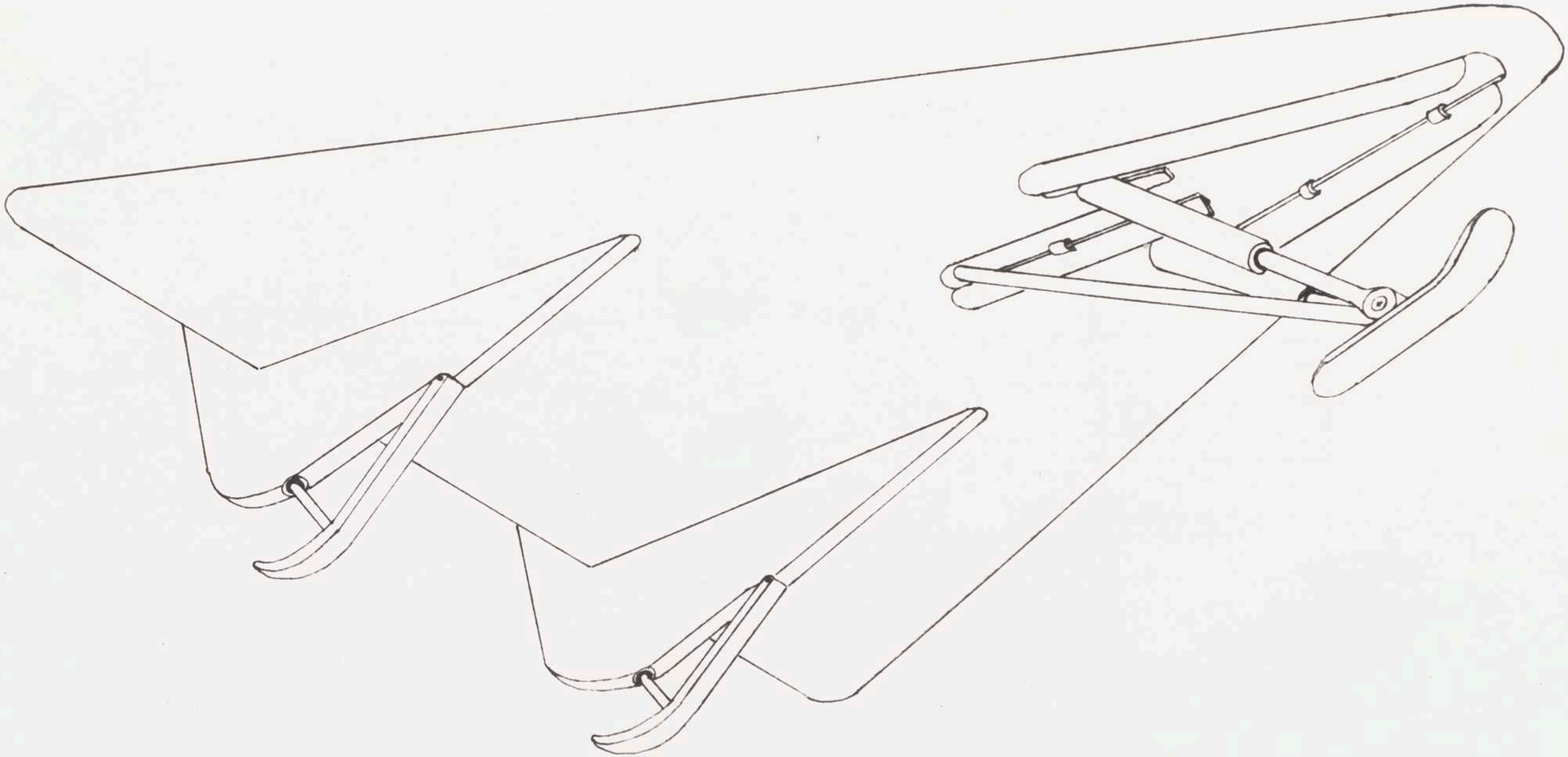

CONFIGURATION I SHOWN READY FOR LANDING WITH GEAR FULLY EXTENDED

FIG. 8c

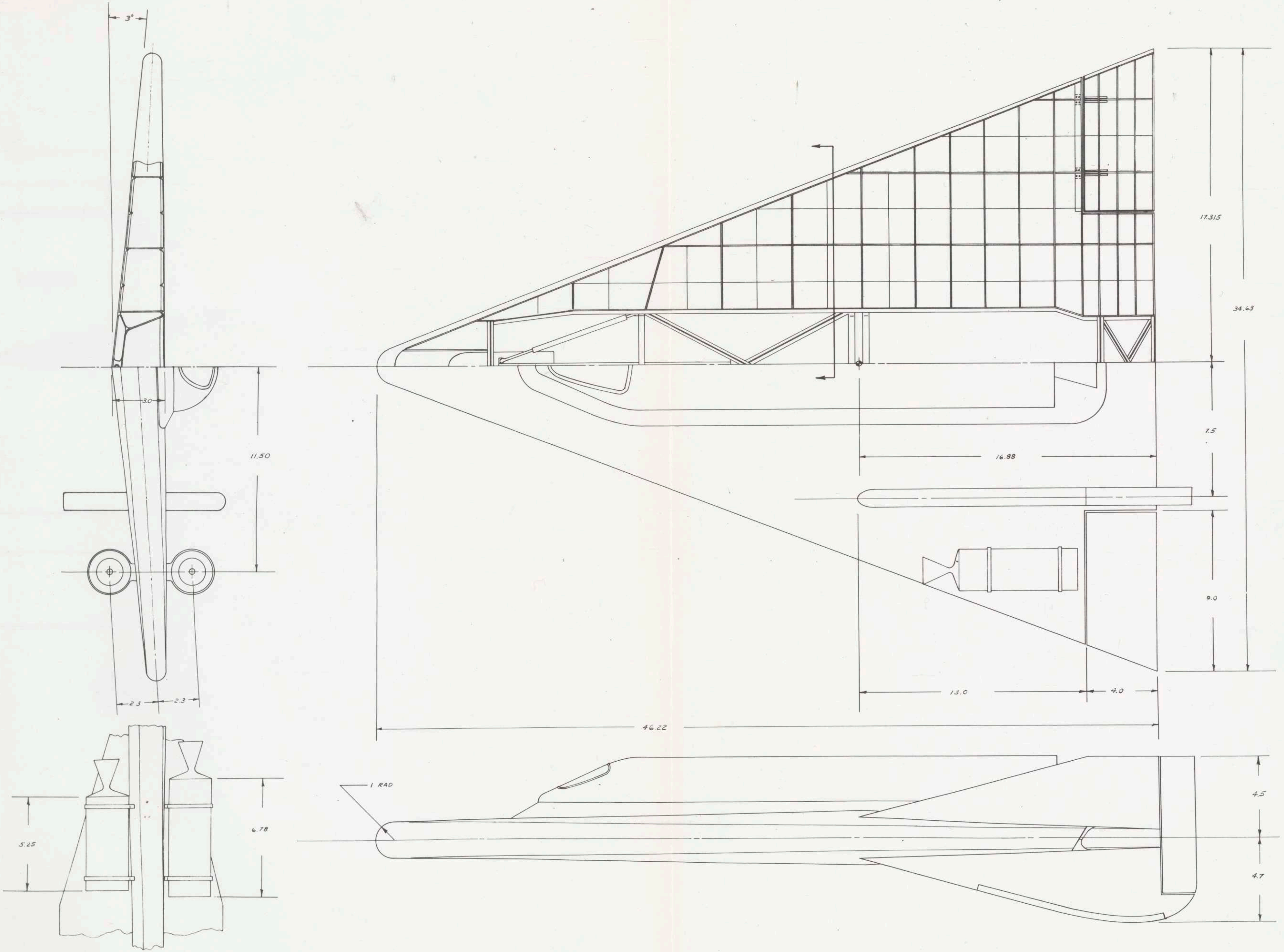

LAYOUT OF CONFIGURATION I

FIG. 9c

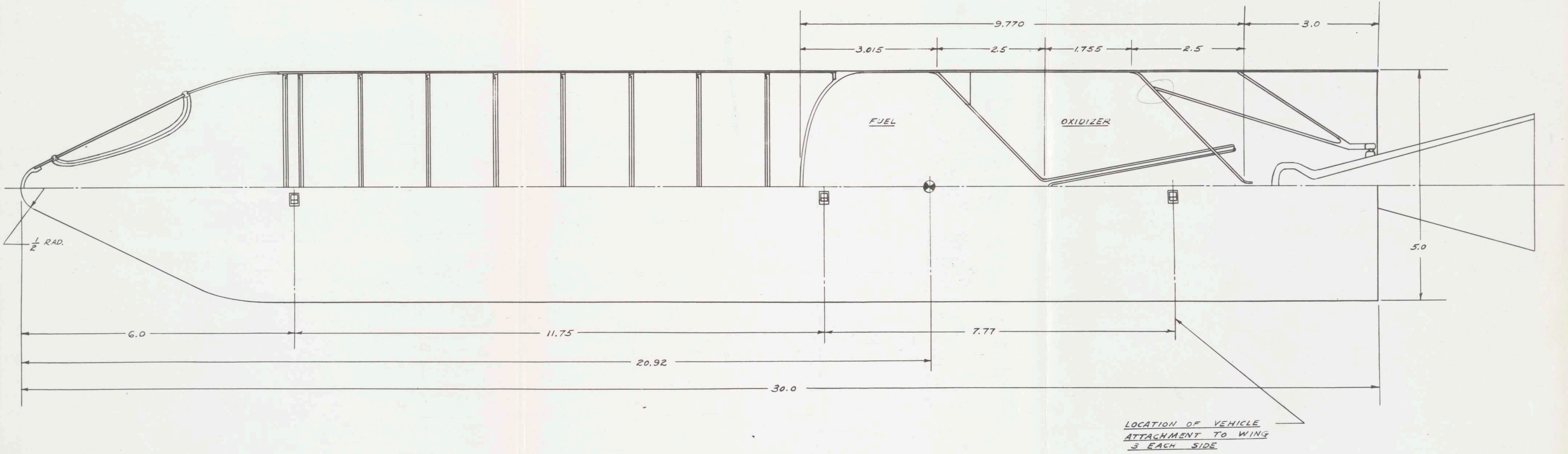

LAYOUT OF CONFIGURATION II

FIG. 10c

PULL OUT →

SKETCHES OF SOME CONSTRUCTION DETAILS

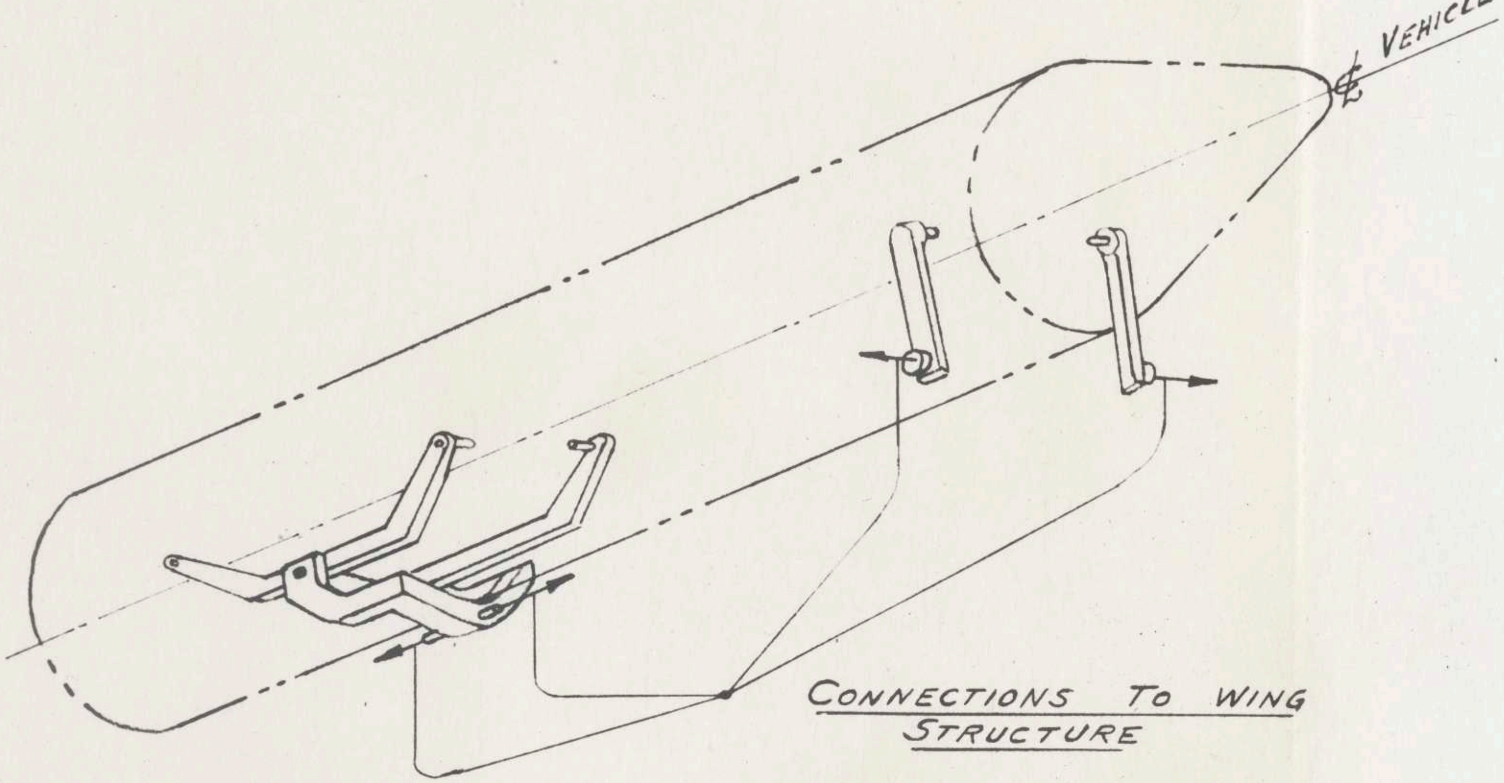

VEHICLE IN HORIZONTAL POSITION SHOWING TIE-IN MECHANISM TO WING STRUCTURE

FIG. 11-C

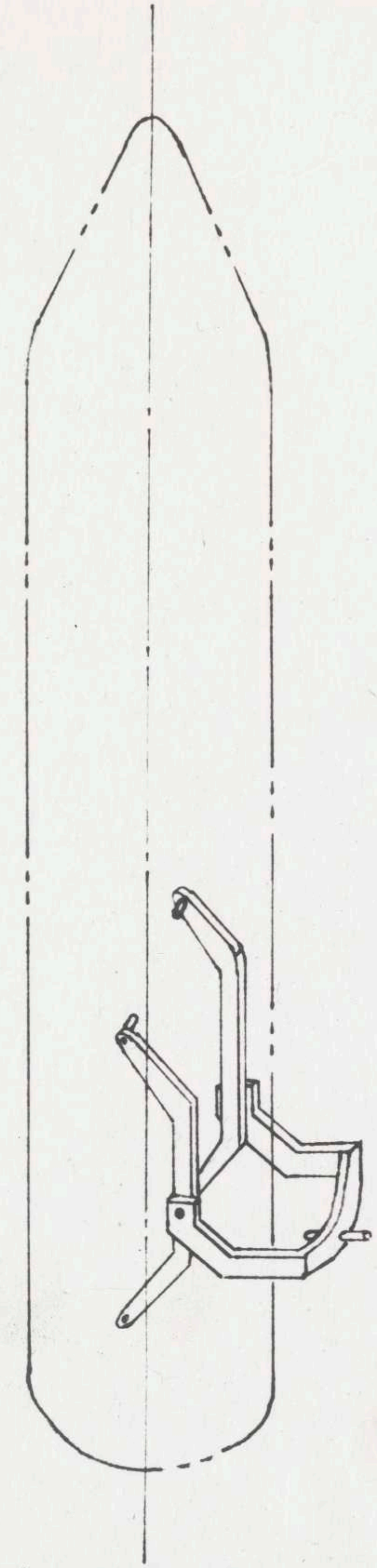

VEHICLE ERECTED TO VERTICAL POSITION

FIG. 12-C

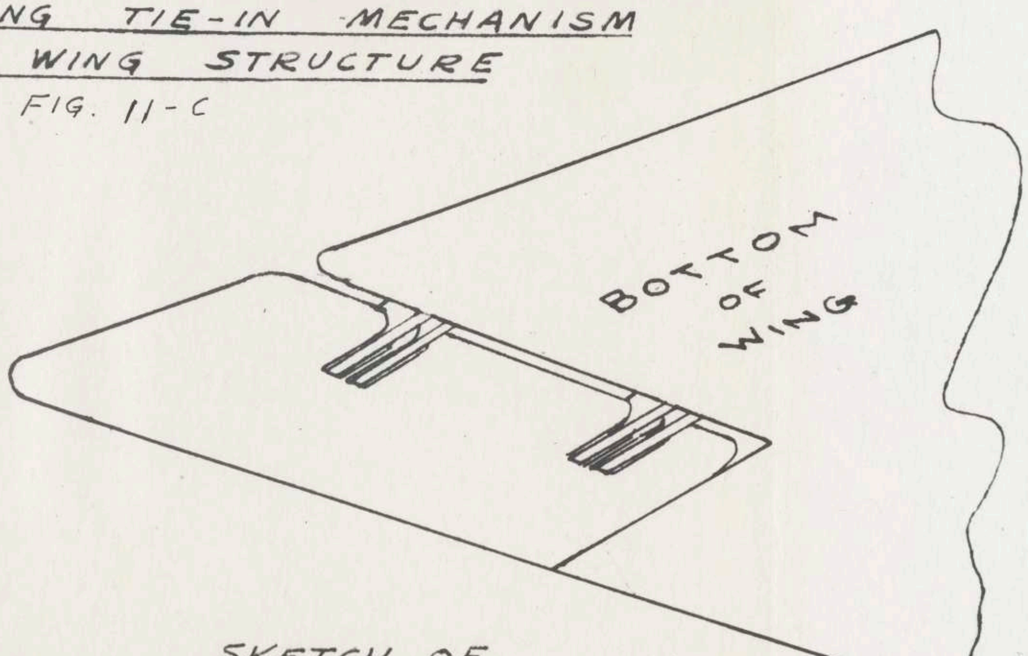

SKETCH OF ELEVON & HINGE MECHANISM

FIG. 13-C

CHAPTER IV

PROPULSION DESIGN

SYMBOLS:

A	area
$\bar{c}$	average liquid specific heat, Btu/lb° F
	of ideal exhaust velocity
C_d	discharge coefficient
C_F	thrust coefficient
d	density
D	diameter
F_T	thrust, lb.
g_o	acceleration of gravity (32.2 ft^2/sec)
I_{sp}	specific impulse lb/lb-sec
k	specific heat ratio
l	length of cylindrical portion of combustion chamber, in.
M_c	average molecular weight of combustion products
MR	mass ratio
P	pressure
ΔP	change of pressure
$\bar{q}$	average heat transmission rate per unit area Btu/sec ft^2
Q	volume flow, ft^3/sec
r	mixture ratio, lb oxidizer/lb fuel
R'	universal gas constant (1544 ft-lb/°R mole)
T	temperature
t_p	burning time, sec.
v	velocity, ft/sec
v_p	velocity at end of burning ft/sec
V	specific volume, ft^3/lb
$\dot{w}$	propellant weight flow rate, lb/sec
W_p	propellant weight, lb
x	length of converging cone of combustion chamber, in.

GREEK SYMBOLS:

γ	angle of injection stream, degrees
ξ_F	thrust correction factor
ξ_v	velocity correction factor
ρ	density, lb/in^2

SUBSCRIPTS:

a	ambient
a_o	atmospheric, sea-level
c	combustion chamber
e	nozzle exit
f	fuel (UDMH)
o ox	oxidizer (IRFNA)
P	propellant
t	throat
2	nozzle exit (ideal)

ASCENT VEHICLE ROCKET PROPULSION SYSTEM

The method of calculating specifications for the rocket engine is taken from Sutton,(Ref. 22) and Shapiro, Vol. I (Ref. 21). For the propellants used and the thrust necessary, it is reasonable to assume a chamber pressure of 600 psia. The engine will have to operate in an atmosphere and in a vacuum, therefore for optimum overall performance it is necessary to expand to half of standard sea-level pressure at the nozzle exit. Human requirements for acceleration factors will be the design criteria for the rocket thrust. It was decided that the maximum acceleration the crew can tolerate and still remain reasonably functional is 3.23 Earth g's. This acceleration will occur during the final thrusting maneuver adopting to satellite orbit when the mass of the vehicle is at it's lowest value. Due to satellite rendezvous requirements on the control system, the rocket engine should be designed for variable thrust. (Ref. 76 & 84) However, this represents problems beyond the scope of this thesis, so the engine will be designed for constant thrust. Terminal guidance will have to be accomplished by very accurate control of burning time.

Propellants:		IRFNA & UDMH
Exit Pressure:	P_e =	0.62 psia
Atmospheric Pressure:	P_{a_o} =	1.24 psia
Chamber Pressure:	P_c =	600 psia
Thrust:	F_T =	6600 lbs

Propellant characteristics:

r	2.6	
T_c	5200° F (5660° R)	
k	1.23	
M_c	22	
d	1.23 g/cc = 76.8 lb/ft^3	
d_{IRFNA}	1.60 g/cc = 99.9 lb/ft^3	
d_{UDMH}	0.768 g/cc = 48.0 lb/ft^3	
I_{SP}	306 sec	(See Appendix IV)

Calculating exhaust velocities and flow rates we get:

$$v_2 = I_s g_0 = 9860 \text{ ft/sec} \tag{1f}$$

$$\bar{c} = \zeta_v v_2 = 9260 \text{ ft/sec} \qquad \zeta_v = 0.94 \tag{2f}$$

$$\dot{\omega}_p = \frac{F_T g}{\bar{c}} = 22.94 \text{ lb/sec} \tag{3f}$$

$$\dot{\omega}_{ox} = 16.57 \text{ lb/sec} \tag{4f}$$

$$\dot{\omega}_{FUEL} = 6.37 \text{ lb/sec} \tag{5f}$$

$$t_p = \frac{W_p}{\dot{\omega}_p} \quad 499.3 \text{ sec} \tag{6f}$$

Thrust chamber design specifications:

Cylindrical combustion chamber.
Helically wound cooling coil with one of propellants as coolant.
Multiple hole injector with injector pressure drop of 100 psia.

(1) NOZZLE CONFIGURATION:

$$C_F = \sqrt{\frac{2K^2}{K-1}\left(\frac{2}{K+1}\right)^{\frac{K+1}{K-1}}\left[1-\left(\frac{P_e}{P_c}\right)^{\frac{K-1}{K}}\right]} + \frac{P_e - P_a}{P_c}\,\frac{A_e}{A_t} \tag{7f}$$

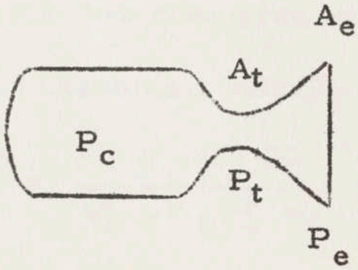

$C_{F_{opt.}}$ 1.77

(p. 68 Sutton, Ref. 22)

$$\frac{P_c}{P_a} = 484$$

We have to get A_e / A_T so:

$$F_T = \mathcal{S}_F \, c \, \frac{\dot{\omega}}{g} = \mathcal{S}_F F_i = \mathcal{S}_F C_F P_c A_T \qquad \mathcal{S}_F = 0.96 \tag{8f}$$

$$A_t = \frac{F/\mathcal{S}_F}{C_F P_c} = 6.47 \text{ sq. in.}$$

$$D_t = \sqrt{\frac{4 A_t}{\pi}} = 2.87 \text{ in.}$$

Solving by iteration for C_F, we get:

$$C_F = 1.804 + (\text{term due to } A_e / A_t)$$

We can solve for the exit area of the nozzle by the continuity equation.

$$\dot{\omega}_x = \dot{\omega}_y = \frac{A_x v_x}{V_x} = \frac{A_Y v_Y}{V_Y} \tag{9f}$$

$$A_e = \frac{\dot{\omega} V_e}{\bar{c}} = \frac{F_T g V_c}{\bar{c}^2} \left(\frac{P_c}{P_e}\right)^{\frac{1}{K}} = \frac{F_T g T_c R'}{\bar{c}^2 P_c M_c} \left(\frac{P_c}{P_e}\right)^{\frac{1}{K}} \tag{10f}$$

$A_e = 917$ sq. in. $\qquad D_e = 34.15$ in. $\qquad C_F = 1.474$ (at sea level)

Summary of nozzle specifications:

Throat area	6.47 sq. in.
Exit area	917 sq. in.
Throat diameter	2.87 in.
Exit diameter	34.15 in.
Nozzle diffuser half angle	15°
Exhaust velocity	9260 ft/sec
Nozzle length	58.4 in.

(2) CHAMBER CONFIGURATION:

Chamber velocities are not readily calculated or measured. They are generally low compared to nozzle velocities. (approx. 200-400 ft/sec.) Assume a velocity of 250 ft/sec.

$$A_c = \frac{\dot{\omega} V_e}{v_c} = \frac{F_T g R' T_c}{v_E M_c P_c v_c} = 60.8 \text{ sq. in.} \tag{11f}$$

Chamber diameter $D_c = 8.795$ in.

$L^* = V_c/A_t$ length of rocket of same volume if it were a straight tube

$L^* = 60$ (good value for our liquid propellants)

$V_c = L^* A_t$

Chamber diameter	D_c =	8.8 in.
Chamber area	A_c =	61 in^2
Convergence angle		30^o
Chamber volume	V_c =	390 $in.^3$
Length of cyl. chamb. portion	l =	3.88 in.
Length of converging cone	x =	7.62 in.
Cone volume		154.5 in^3
Cylindrical volume		235.5 in^3

For a diagram of the complete rocket engine configuration see figure 1e.

(3) HEAT TRANSFER:

The thrust chamber is to be regeneratively cooled. Calculating approximate heat transfer fimm coefficients of the gas layer is somewhat questionable because of the usual poor accuracy of these calculations. Also it was impossible to find data concerning coefficients of viscosity, accurate densities, and specific heat coefficients at different temperatures. Accurate heat transfer data will have to be determined by tests. The average wall temperature of the chamber will not be calculated, and the cooling jacket for the rocket will not be designed due to lack of sufficient data. However, the average temperature rise of the coolant will be calculated by assuming an average heat flow of 0.6 Btu/in^2 sec. This is absorbed by the coolant. It is impossible to use the UDMH for the coolant beaause of its low flow rate and its low boiling temperature. The areas for heat flow are:

A_S	(chamber)	107 sq. in.
A_S	(Conic diffuser)	122
A_S	(nozzle)	3540
	A_S total	3769 sq. in.

Total heat transfer $\quad Q = A\ \bar{q} = 1885$ Btu/sec (12f)

Using IRFNA for the coolant we get the mean coolant temperature rise as:

$$\Delta T = \frac{A\ \bar{q}}{\dot{w}_f\ \bar{c}} = 167.4^{\circ}\ F. \tag{13f}$$

Assuming the temperature of the propellant in the tanks at take-off is 0° F., the temperature of the coolant leaving the cooling jacket is 167° F. It is concluded that it would probably be unfeasible to attempt to cool the engine with UDMH flow through the coolant jacket. IRFNA will be used for this purpose.

(4) INJECTOR DESIGN:

The injectors are arbitrarily chosen as a multiple-hole impinging jet inj ector because such injectors have given good performance in the past. There will be 20 pairs of injection streams, each consisting of an oxidizer and a fuel jet, with the resultant momentum of each jet pair in the axial direction.

$\dot{w}_p = 22.94$ lb/sec $\qquad \dot{w}_{ox} = 16.57$ lb/sec

$\qquad\qquad\qquad\qquad\qquad \dot{w}_f = 6.37$ lb/sec

The following quantities and properties are of concern:

	UDMH	IRFNA
Temp. of injected propellant	130° F.	168° F.
Density at injection temp.	45 lb/ft^3	90 lb/ft^3
Heat of vaporization at STP	100 BTu/lb	115 Btu/lb
Boiling pt. at 1 atm. (earth)	146° F.	187° F.
Specific heat of injected prop.	0.70	0.95

It is assumed that the eemperature at takeoff of the propellants will be 0° F.

The propellant injection volume flows are:

$$Q_o = \frac{\dot{\omega}_o}{\rho_o} = \quad 318\ in^3/sec$$

$$Q_f = \frac{\dot{\omega}_f}{\rho_f} = \quad 245\ in^3/sec$$

We will calculate the injector hole areas from:

$$\sum A_o = \frac{\dot{\omega}_o}{C_d\sqrt{2g\,\Delta P\,\rho_o}} \tag{14f}$$

It is assumed that the injection pressure drops in the fuel and oxidizer lines are equal to 100 psia., and that both orifice discharge coefficients are equal to 0.75.

$A_o = 0.348\ in^2$ $\qquad$ $A_f = 0.1895\ in^2$

There are twenty pairs of injectors, so the individual hole areas and diameters will be:

A_o	0.0174 sq. in.	A_f	0.00925 sq. in.
D_o	0.1487 in.	D_f	0.1085 in.
D_o	0.01755		

For construction of these injectors we will use Drill #25 for drilling the oxidizer holes, and Drill #35 for drilling the fuel holes. If we assume no jet contraction, then the injection velocities will be:

$$v = C_d\sqrt{\frac{2g\,\Delta P}{\rho}} \tag{15f}$$

$v_f = 118.5$ ft/sec $\qquad$ $v_o = 76.1$ ft/sec

These velocities have magnitudes which promise to give good injection and justify the original assumption of 100 psi injection drop.

The injection angles are now to be chosen so that the resultant momentum will be in an axial direction. This is done in accordance with equation: $\dot{w}_o v_o \sin\gamma_o = \dot{w}_f v_f \sin\gamma_f$, and by arbitrarily selecting the angle of inclination of the oxidizer jet at 20 degrees.

$$\sin\gamma_f = \frac{\omega_o V_o}{\omega_f V_f}\sin\gamma_o \tag{16f}$$

$$= 0.57 \qquad \gamma_f = 34.75^\circ$$

The following quantities have now been determined for the injector:

Injector Design Parameter	Fuel	Oxidizer
Flow (total propellant flow = 22.94 $\frac{lb}{sec}$)	6.37 lb/sec	16.57 lb/sec
Volume flow	245 in^3/sec	318 in^3/sec
Pressure drop through Injector	100 psi	100 psi
Injection velocity	118.5 ft/sec	76.1 ft/sec
Number of Injection holes	20	20
Diameter of each hole	o.1100 in.	0.1495 in.
Angle of hole with nozzle axis	34.75°	-20°
Total injection area	0.1895 in^2	0.348 in^2

(5) TURBOPUMP DESIGN:

The turbopump design will be for a gas bleeding system for driving the turbine, using gas direct from the main combustion chamber. This gas will have to be fed into a heat exchanger in order to cool it to temperatures necessary for turbine operation. Compressed air will be used to start the turbines initially. The thrust gases will be cooled by the UDMH flow in the heat exchanger.

Turbine design:

The turbine will be constructed from Inconel X. It will be run at 1600° F. At this temperature, $U.S._T = 23,000$ psi. Flow rate of gas through the turbine is estimated as 0.40 lb/sec.

Heat exchanger:

The gas from the thrust chamber has to be cooled from 4600° F to 1600° F, a drop of 3000° F. The heat flow from the gas is:

$$A\bar{q} = T_{gas}\bar{w}_f\bar{c} = 197 \text{ Btu/sec} \tag{17f}$$

So the rise in temperature of the UDMH will be:

$\Delta T_{UDMH} = 43°$ for full UDMH flow rate through the heat exchanger.

RETRO_ROCKETS

Retro-rockets will have to be employed to reduce the vehicle's speed from circular orbit velocity to the velocity needed for the transfer orbit. For our configuration, aerodynamic braking to keep the vehicle within the atmosphere is impossible, due to the high temperatures encountered in this maneuver. Therefore, another set of retro-rockets will have to be used for this task.

The retro-rockets are mounted on the exterior of the wing and are jettisoned at burnout. The device for jettisoning the rockets can be a cylinder operated from a gas-charged accumulator. This ensures that the burned-out rocket cases will be ejected sufficiently far away to minimize the hazard of damaging the structure of the vehicle. Mounts for the rockets will produce no net moment about the vehicle's center of mass. The retro-rockets are end-burning solid rockets. The fuel is assumed to have a specific impulse of 250 seconds. It is also assumed that the structural factor, ϵ , for the rocket cases is 5%. We will also assume the following characteristics for the solid fuel propellant:

Burning rate 0.30 in/sec @ 1000 psi and 70° F.

Specific weight 0.055 lb/in^3

Operating temperature limits -70 to 170° F.

In order to calculate the weights of the retro-rockets, we will use the following formulas:

(1e)

(2e)

$$v_2 = I_{sp} g_o = 8050 \text{ ft/sec} \tag{1e}$$

$$\bar{c} = \mathcal{f}_v v_2 = 7560 \text{ ft/sec} \tag{2e}$$

$$v_p = \bar{c} \ln MR \tag{3e}$$

We will define retro-rockets I as the two rockets used to establish the transfer orbit, and retro-rockets II as those used to adopt the vehicle to the circular orbit at an altitude of 700,000 feet. The results of the weight calculations are.

	Retro I	Retro II
Total propellant weight	4370 lb	4190 lb
Total structural weight	214	210
Total thrust	235	235

DESIGN OF RETRO-ROCKET I (2 Units):

Each rocket will weigh 2685 pounds. The volume and dimensions for the units were then determined as follows.

$$Vol_1 = \frac{W_p}{\rho_p} = 28.2 \text{ ft}^3$$

$\dot{\omega}_p$ = Burning rate x cross-sectional areax specific weight.

Solving for cross-sectional area and solving for the diameter give:

$$D_1 = 2.32 \text{ feet}$$

and length of unit $L_1 = 6.73$ feet.

DESIGN OF RETRO-ROCKET II (2 units).

Each rocket will weigh 2095 pounds. Calculations were carried out similar to those used for Rocket I and the following results were obtained:

$Vol_2 = 22.05\ ft^3$

$D_2 = 2.32\ ft$

$L_2 = 5.25\ ft.$

CONSTRUCTION OF ROCKET CASES:

The cases for both sets of rockets are to be made exactly the same. They are to be made of 7075ST6 aluminum alloy whose density is 0.101 lb/in^3 which gives a wall thickness of 0.0980 in. for Rockets I and 1.20 in. for Rocket II. This allows a 0.10 inch think plate at the end of each case and 30 lbs. of material for the construction of the nozzles and supports. Hoop stress calculations showed that the maximum stress in the case was about 70,000 psi which is acceptable. See Figure 9c for a drawing of the rocket cases.

MOUNTING OF THE RETRO-ROCKETS:

The rockets will be mounted in pairs on top and bottom of the wing on opposite sides of the wing center line. When arranged in this manner there will be no moment created about the configuration C.G. due to the thrusting maneuver.

Retro-rockets for the initial thrusting will be carried on the upper left hand and lower right hand wing surfaces. The unbalanced moment after ejection of the first set of retro-rockets will be accomplished by a gas-jet control system which will have to be installed for vehicle attitude control while outside the atmosphere.

CROSS SECTION OF ASCENT VEHICLE ROCKET MOTOR

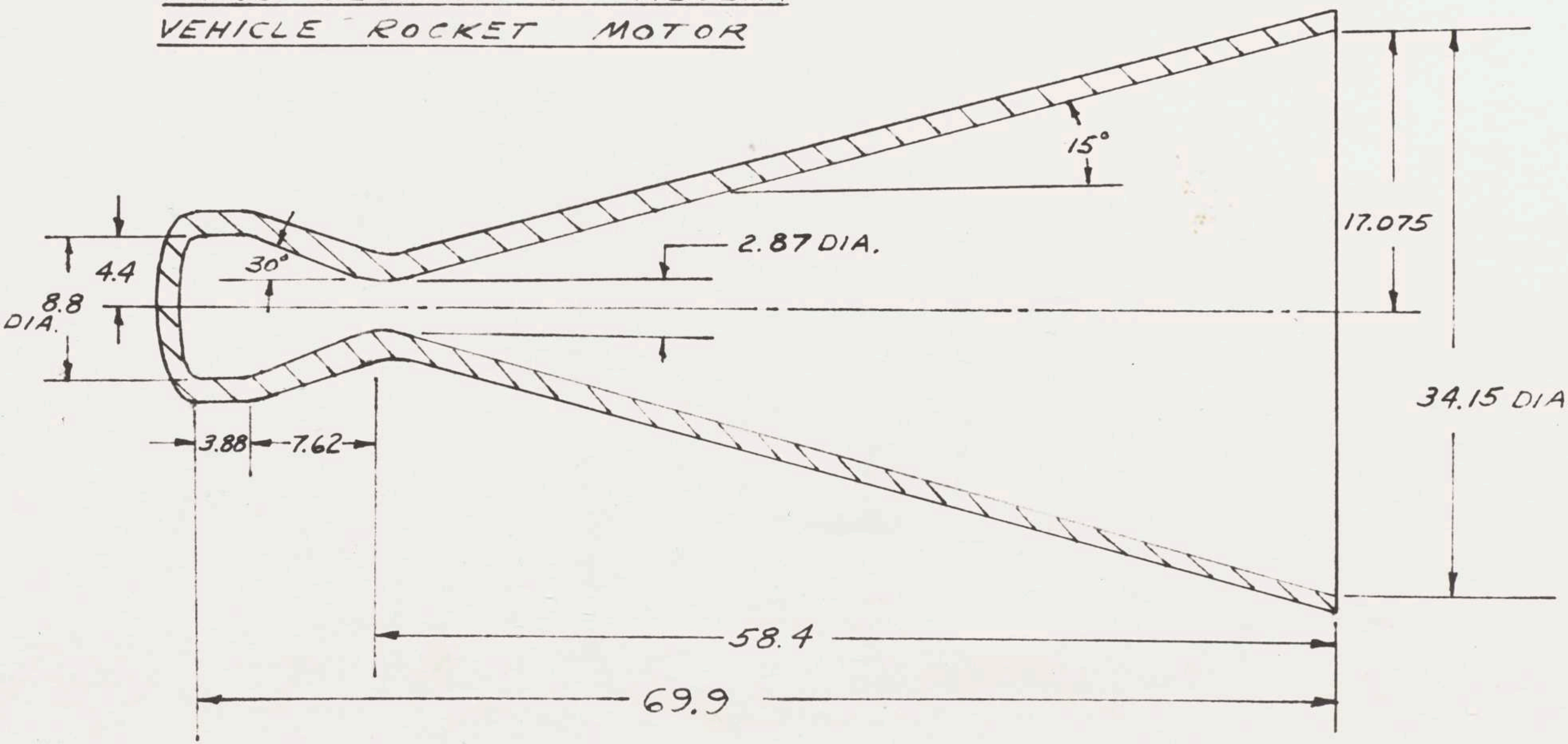

FIG. 1e

BIBLIOGRAPHY

BOOKS:

1. Alperin, Stern, & Wooster, editors. Vistas in Astronautics. New York: Pergamon Press. 1958.

2. Bisplinghoff, Ashley, & Halfman. Aeroelasticity. Cambridge: Addison-Wesley Publishing Co., Inc., 1955.

3. Bonney, E. Arthur. Engineering Supersonic Aerodynamics. New York: McGraw-Hill Book Co., Inc., 1950.

4. De Vaucoulers, Gerard. Physics of the Planet Mars. London: Faber and Faber Limited, 1954.

5. Etkin, Bernard. Dynamics of Flight. New York: John Wiley & Sons, Inc. 1959.

6. Hoerner, Sighard F. Fluid-Dynamic Drag. Midland Park, N.J.: Published by Author, 1958.

7. Kuiper, Gerard P., editor. The Atmospheres of the Earth and Planets. Chicago: The University of Chicago Press, 1957.

8. Ley & von Braun. The Exploration of Mars. New York: The Viking Press, 1956.

9. Liepmann & Roshko. Elements of Gas Dynamics. New York: John Wiley & Sons, Inc., 1957.

10. Moore, Patrick. Guide to Mars. New York: The Macmillan Co., 1958.

11. Moulton, Forest Ray. An Introduction to Celestial Mechanics. New York: The Macmillan Co., 1958.

12. Niles & Newell. Airplane Structures. Vol I. New York: John Wiley & Sons, Inc., 1954.

13. Nixon, Floyd E. Principles of Automatic Controls. Englewood-Cliffs, N.J.: Prentice-Hall, Inc., 1956.

14. Peery, David J. Aircraft Structures. New York: McGraw-Hill Book Co., Inc., 1950.

15. Perkins, Courtland D. & Hage, Robert E. Airplane Performance, Stability and Control. New York: John Wiley & Sons, Inc., 1957.

16. Rauscher, Manfred. Introduction to Aeronautical Dynamics. New York: John Wiley & Sons, Inc., 1953.

17. Russell, Dugan, & Stewart. Astronomy. Boston: Ginn & Co., 1945.

18. Schniearbeit, Prof. C. S. Thesis Writing. Chicago: Schuh Typesetting Co., 1937.

19. Sechler & Dunn. Airplane Structural Analysis and Design. New York: John Wiley & Sons, Inc., 1942.

20. Shanley, F. R. Strength of Materials. New York: McGraw-Hill Book Co., Inc., 1957.

21. Shapiro, Ascher H. The Dynamics & Thermodynamics of Compressible Fluid Flow. Vol. I & II. New York: The Ronald Press Co., 1953.

22. Sutton, George P. Rocket Propulsion Elements. New York: John Wiley & Sons, Inc., 1956.

23. Timoshenko, S. Theory of Plates and Shells. New York: McGraw-Hill Book Co., Inc., 1940.

24. Truxal, John G. Automatic Feedback Control System Synthesis. New York: McGraw-Hill Book Co., Inc., 1955.

25. von Braun, Wernher. The Mars Project. Urbana: The University of Illinois Press, 1953.

26. Warren, Francis A. Rocket Propellants. New York: Reinhold Publishing Corporation, 1958.

27. Zucrow, M. J. Aircraft & Missile Propulsion. Vol I. Thermodynamics of Fluid Flow and Application to Propulsion Engines. New York: John Wiley & Sons, Inc., 1958.

28. Zucrow, M. J. Aircraft & Missile Proplusion. Vol II. The Gas Turbine Power Plant, The Turboprop, Turbojet, Ramjet, and Rocket Engines. New York: John Wiley & Sons, Inc., 1958.

HANDBOOKS:

29. Aeronautical Vest-Pocket Handbook. Pratt & Whitney Aircraft, '57.

30. Alcoa Structural Handbook. Pittsburgh: Aluminum Co. of America 1956.

31. Burington, Richard Stevens. Handbook of Mathematical Tables and Formulas. Sandusky, Ohio: Handbook Publishers, Inc., 1955.

32. Hodgmen, Charles S., editor. C.R.C. Standard Mathematical Tables. Cleveland: Chemical Rubber Publishing Co., 1957.

33. Hodgmen, Charles S., editor. Handbook of Chemistry & Physics. Cleveland: Chemical Rubber Publishing Co., 1954.

34. Keenan & Kaye. Gas Tables. New York: John Wiley & Sons, Inc. 1956.

35. Lange, Norbert Adolph, editor. Handbook of Chemistry. Sandusky, Ohio: Handbook Publishers, Inc., 1956.

NACA REPORTS:

36. Becker, Herbert. Buckling of Composite Elements. NACA TN 3782 1957.

37. Abbott, Doenhoff, & Stivers. Summary of Airfoil Data. Rep. 824. 1945.

38. Chapman, Dean R. An Approximate Analytical Method for Studying Entry Into Planetary Atmospheres. NACA TN 4276.

39. Brown, Clinton E. Theoretical Lift and Drag of Thin Triangular Wings at Supersonic Speeds. NACA Rep. 839, 1946.

40. Gerard, George, & Becker, Herbert. Buckling of Flat Plates. NACA TN 3781, 1957.

41. Gerard, George, & Becker, Herbert. Buckling of Curved Plates and Shells. NACA TN 3783, 1957.

42. Gerard, George. Failure of Plates and Composite Elements. NACA TN 3784, 1957.

43. Gerard, George. Compressive Strent th of Flat Stiffened Panels. NACA TN 3785, 1957.

44. Jones, Robert T. Properties of Low-Aspect-Ratio Pointed Wings at Speeds Below and Above the Speed of Sound. NACA Rep 835 1946.

45. Jones, Sorenson, & Lindler. The Effects of Sideslip, Aspect Ratio, and Mach Number on the Lift and Pitching Moment of Triangular, Trapezoidal, and Related Plan Forms in Supersonic Flow. NACA TN 1916, 1949.

46. Love, Eugene S. Investigations at Supersonic Speeds of 22 Triangular Wings Representing Two Airfoil Sections For Each of 11 Apex Angles. NACA Rep. 1238, 1955.

47. Nielsen, Goodwin, & Mersman. Three-Dimensional Orbits of Earth Satellites, Including Effects of Earth Oblateness and Atmospheric Rotation. NASA Memo 12-4-58A, 1958.

48. Tobak & Allen. Dynamic Stability of Vehicles Traversing Ascending or Descending Paths Through the Atmosphere. NACA TN 4275, 1958.

MISCELLANEOUS REFERENCES:

49. Adams, Mac C. & Camac, M. The Arc Heated Plasma Thrust Chamber. ARS Rep. 791-59, 1959.

50. Berman, Lawrence J. The Correction of Epoch Error in Circular Orbits. ARS Rep. 792-59, 1959.

51. Blazek, Henry F. The Performance of Inertial Guidance Components on an Unstabilized Base. ARS Rep. 775-59, 1959.

52. Brady, George. Application and Uses of Satellites. ARS Rep. 783-59, 1959.

53. Crocco, G. A. One-Year Exploration Trip. Earth-Mars-Venus-Earth. Associazione Italian Razzi: Comptes Rendus du VII Congres Astronautique International, p. 175. Rome: 17-22 Septembre 1956.

54. Detra, Riddell, & Rose. Controlled Recovery of Non-Lifting Satellites. ARS Rep. 784-59, 1959.

55. Edward, & Brown. Ion Rockets for Small Satellites. ARS Rep. 789-59, 1959.

56. Ehricke, Kraft A. A New Supply System for Satellite Orbits. Part 1, p. 303; Part 2, p. 369. Satellite Orbits for Interplanetary Flight. p. 381. Jet Propulsion Vol. 24, 1954.

57. Ehricke, Kraft A. Aero-Thermodynamics of Descending Orbital Vehicles. p. 1. Astronautica Acta, 1956.

58. Ehricke, Kraft A. Ascent of Orbital Vehicles. p. 175. Astronautica Acta, 1956.

59. Ehricke, Kraft A. Analysis of Orbital Systems. P. 18. Wien/Innsbruck: Bericht uber den V. Internationalen Astronautischen Kongreb. Innsbruck: 5. bis 7, 1954.

60. Ehricke, Kraft. A. On the Descent of Winged Orbital Vehicles. p. 137. Astronautica Acta, 1955.

61. Ehricke, Kraft A. Space Flight. Chapter 3, The Solar System. Convair-Astronautics Rep. AZM-008, 1957.

62. Harris, Suer, Skene, & Benjamin. The Stability of Thin-Walled Unstiffened Circular Cylinders Under Axial Compression Including the Effects of Internal Pressure. I.A.S. Preprint No. 660, 1957.

63. Kepler, Donald I. Concepts Influencing the Selection of a Configuration for Atmospheric Re-entry. ARS Rep. 786-59, 1959.

64. King-Hele, D. G., & Gilmore, D. M. C. The Effect of the Earth's Oblateness on the Orbit of a Near Satellite. Tech. Note G.W. 475. London: 1957.

65. Klund, Edelbaum, & Podolny. Propulsion Systems for Controlling Satellite Orbits. ARS Rep. 788-59, 1959.

66. Kooy, J.M.J. Thermodynamic Theory of Rocket Motors with Hydrazine and Nitric Acid as Fuels. p. 157. Astronautica Acta, 1955.

67. Kupperian, J. E. Electromagnetic Radiation Environment. ARS Rep. 780-59, 1959.

68. Larrabee, Eugene. 16.13 Class Notes: Aircraft Stability and Control. 1958, M.I.T.

69. Larrabee, Eugene. 16.15 Class Notes: Advanced Aircraft Stability and Control. M.I.T. 1959.

70. Lawden, D.F. Optimum Launching of a Rocket Into an Orbit About the Earth. p. 185. Astronautica Acta, 1955.

71. Lees, Hartwig, & Cohen. The Use of Aerodynamic Lift During Entry Into the Earth's Atmosphere. ARS Rep. 785-59, 1959.

72. Miele, A. General Variational Theory of the Flight Paths of Rocket-Powered Aircraft, Missiles, & Satellite Carriers. p. 264. Astronautica Acta, Vol. IV/Fasc. 4, 1958.

73. Miele, & Cavoti. Optimum Thrust Programming Along Arbitrarily Inclined Rectilinear Paths. p. 167. Astronautica Acta, Vol. IV/Fasc. 3, 1958.

74. Minzner, R.A. Higher Atmospheric Densities and Temperatures Demanded by Satellite and Recent Rocket Measurements.

75. Moness, Elias. Flat Plates Under Pressure. Journal of the Aeronautical Sciences. Vol. 5, No. 11, p. 421, 1938.

76. Nason, Martin L. Terminal Guidance and Rocket Fuel Requirements for Satellite Interception. ARS Rep. 777-59, 1959.

77. Orbital and Satellite Vehicles. Vol. 1. M.I.T. Aero. Dept. Notes. 1958.

78. Orbital and Satellite Vehicles. Vol. 2. M.I.T. Aero. Dept. Notes. 1958.

79. Rocket Engine Propellants. Pub. 505-X. Rocketdyne, A Division of North American Aviation, Inc., 1956.

80. Sandorff, Paul E. 16.76 Class Notes: Satellite and Orbital Vehicles. 1959.

81. Sandorff, Paul E. Structures for Spacecraft. ARS Paper 733-58, 1958.

82. Sanscrainte, & Schiavone. Rocket Systems for Satellite Attitude Control. ARS Rep. 790-59, 1959.

83. Schlager, & Young. A Guidance Approach to Earth Satellite Orbit Modification. ARS Rep. 776-59, 1959.

84. Sears, & Felleman. Terminal Guidance for Satellite Rendezvous. ARS Rep. 778-59, 1959.

85. Singer, S. F. The Corpuscular Radiation Environment of the Earth. ARS Rep. 782-59, 1959.

86. Space Explorers. Jet Propulsion Laboratory, 1958.

87. Strength of Metal Aircraft Elements. Bulletin ANC-5. Washington: U.S. Government Printing Office, 1955.

88. Handbook of Supersonic Aerodynamics. Washington: U.S. Government Printing Officel Vol. 1, 1950; Vol. 2, 1953; Vol. 3, 1957.

89. Tormey, John F. Liquid Rocket Propellants: Is There an Energy Limit? I.A.S. Paper 510-P. New York: 1957.

90. Waul, John K. The Feasibility of Aerodynamic Attitude Stabilization of a Satellite Vehicle. ARS Rep. 787-59, 1959.

91. Whitney, Charles A. Atmospheric Conditions at High Altitudes from Satellite Observations. ARS Rep. 779-59, 1959.

92. VIIth International Astronautical Congress. Proceedings, Barcelona 1957. Wien -- Springer-Verlag, 1958.

93. Henderson, Arthur, jr. Pitching-Moment Derivatives C_{m_q} and C_m at Supersonic Speeds for a Slender-Delta-Wing and Slender-Body Combination and Approximate Solutions for Broad-Delta-Wing and Slender-Body Combinations. NACA TN2553, 1951.

94. Tobak, Murray. Dynamic Stability of Re-Entry Vehicles. p. 32, Astronautics, March, 1959.